Journal Pre-proofs


# 3D printed pH-responsive tablets containing N-acetylglucosamine-loaded methylcellulose hydrogel for colon drug delivery applications

Maryam Asadi, Zeinab Salehi, Mohammad Akrami, Mohammadreza Hosseinpour, Stefan Jockenhövel, Samaneh Ghazanfari

PII: S0378-5173(23)00787-1
DOI: https://doi.org/10.1016/j.ijpharm.2023.123366
Reference: IJP 123366

To appear in: *International Journal of Pharmaceutics*

Received Date: 12 May 2023
Revised Date: 31 August 2023
Accepted Date: 1 September 2023

Please cite this article as: M. Asadi, Z. Salehi, M. Akrami, M. Hosseinpour, S. Jockenhövel, S. Ghazanfari, 3D printed pH-responsive tablets containing N-acetylglucosamine-loaded methylcellulose hydrogel for colon drug delivery applications, *International Journal of Pharmaceutics* (2023), doi: https://doi.org/10.1016/j.ijpharm.2023.123366

# 3D printed pH-responsive tablets containing N-acetylglucosamine-loaded methylcellulose hydrogel for colon drug delivery applications

Maryam Asadi [1,4], Zeinab Salehi [1*], Mohammad Akrami [2], Mohammadreza Hosseinpour [3], Stefan Jockenhövel [4,5], and Samaneh Ghazanfari [4,5] *

[1] Department of Biochemical and Pharmaceutical Engineering, School of Chemical Engineering, College of Engineering, University of Tehran, Tehran, Iran
[2] Department of Pharmaceutics, Faculty of Pharmacy, Tehran University of Medical Sciences, Tehran, Iran
[3] Research and Development Department, Naya Life Sciences d.o.o., the Netherlands
[4]Aachen-Maastricht Institute for Biobased Materials, Faculty of Science and Engineering, Maastricht University, the Netherlands
[5] Department of Biohybrid & Medical Textiles (BioTex), AME-Helmholtz Institute for Biomedical Engineering, RWTH Aachen University, Forckenbeckstrabe 55, 52072 Aachen, Germany

**Corresponding authors:**

Samaneh Ghazanfari
Faculty of Science and Engineering, Aachen-Maastricht Institute for Biobased Materials (AMIBM), Maastricht University, Urmonderbaan 22, 6167 RD, Geleen, The Netherlands
Department of Biohybrid and Medical Textiles (BioTex), AME-Helmholtz Institute for Biomedical Engineering, RWTH Aachen University, Forckenbeckstrabe 55, 52072, Aachen, Germany
Samaneh.ghazanfari@maastrichtuniveristy.nl

Zeinab Salehy
Department of Biochemical and Pharmaceutical Engineering, School of Chemical Engineering, College of Engineering, University of Tehran, Tehran, Iran
zsalehy@ut.ac.ir

**Abstract**

The pH-responsive drug release approach in combination with three-dimensional (3D) printing for colon-specific oral drug administration can address the limitations of current treatments such as orally administered solid tablets. Such existing treatments fail to effectively deliver the right drug dosage to the colon. In order to achieve targeted drug release profiles, this work aimed at designing and producing 3D printed tablet shells using Eudragit® FS100 and polylactic acid (PLA) where the core was filled with 100 µL of N-acetylglucosamine (GlcNAc)-loaded methyl cellulose (MC) hydrogel. To meet the requirements of such tablets, the effects of polymer blending ratios and MC concentrations on physical, thermal, and material properties of various components of the tablets and most importantly *in vitro* drug release kinetics were investigated. The tablets with 80/20 weight percentage of Eudragit® FS100/PLA and the drug-loaded hydrogel with 30 mg/ml GlcNAc and 3% w/v MC showed the most promising results having the best printability, processability, and drug release kinetics besides being non-cytotoxic. Manufacturing of these tablets will be the first milestone in shifting from the conventional "one size fits all" approach to personalized medicine where different dosages and various combinations of drugs can be effectively delivered to the inflammation site.

Keywords: 3D printing, colon drug delivery, pH-responsive polymer, controlled release, personalized medicine.

## 1. Introduction

In the past few decades, targeted drug delivery to the colonic region of the gastrointestinal tract has drawn a lot of interest. The desire for more effective treatment of local illnesses of the colon, such as inflammatory bowel disease (IBD) including ulcerative colitis (UC) and Crohn's disease (CD), has sparked research interest in this field (Awad et al., 2022; McCoubrey et al., 2023; Moutaharrik et al., 2021a). IBD of the rectum and sigmoid colon is a frequent condition that usually starts at the rectum and progresses to the left colon before affecting the entire colon and the cecum (Cai et al., 2021). IBD is becoming more widespread worldwide, and since it is still incurable, it has a significant negative impact on patient's quality of life (Dias et al., 2018; Qu et al., 2021). Amino salicylates, antibiotics, corticosteroids, immunomodulators, and biological components are frequently used in the management of IBD. Corticosteroids are frequently used for acute IBD; however, due to their absorption along the upper gastrointestinal tract, contemporary corticosteroid medicines still generate unfavorable systemic side effects (Qu et al., 2021). It is generally recognized that using glucocorticoids to treat IBD can cause steroid dependence, hyperglycemia, glaucoma, cataracts, skin thinning, poor development, and bone density loss (Cai et al., 2021; Qu et al., 2021). IBD is recognized to be influenced by a variety of genetic, immunological, and environmental variables; however, the exact underlying reasons are yet unknown (Cai et al., 2021; Qu et al., 2021). Therefore, the discovery of important mechanisms controlling intestinal inflammation that could be therapeutically targeted is crucial for future advancements in IBD treatment (Dias et al., 2018).

The findings showed that N-acetylglucosamine (GlcNAc) metabolic replenishment of mucosal T cells isolated from individuals with active UC enhanced branched N-glycosylation on the T cell receptor; this was linked to the regulation of T cell activation and function (Dias et al., 2018). GlcNAc can have an impact on cell membranes, intercellular fluids, and cell regeneration (Chen et al., 2010; Dias et al., 2018). With no negative side effects, low costs, and the potential to be used as a straightforward rescue therapy to avoid toxic effects and step-up therapies in IBD, the therapeutic use of GlcNAc, either individually or combined with additional anti-inflammatory treatments, represents a convenient immuno-modulatory strategy in IBD (Chen et al., 2010; Dias et al., 2018). Overall, previous findings presented new opportunities for individualized targeted therapy of GlcNAc for IBD treatment where this component can be administered orally (Chen et al., 2010; Dias et al., 2018). Oral administration offers the highest patient compliance and adherence, which is desirable given that the vast majority of IBD patients need continuous treatment management (Qu et al., 2021).

The conventional manufacturing methods for solid oral dosage forms (SODFs) require numerous operation steps such as blending, mixing, milling and compression. As a consequence, they are time-consuming and highly expensive. Finally, they are not customized to individual needs but are manufactured on a large scale (Charbe et al., 2017; Pitzanti et al., 2022; Sadia et al., 2018). These limitations, however, can be resolved with the aid of the creative and cutting-edge technology known as three-dimensional (3D) printing through specially designed and engineered release patterns, providing a highly individualized pharmacological treatment (Goyanes, Buanz, et al., 2015; Linares et al., 2019; Narala et al., 2023; Ou et al., 2023; Pandey et al., 2020; Pitzanti et al., 2022). The ability to develop almost any dosage amount has made additive manufacturing, more specifically 3D printing, a breakthrough technique in the pharma industry in terms of quality and efficacy, after introducing the first 3D printed tablet into the market approved by the US Food and Drug Administration (FDA) in 2015 (Charbe et al., 2017; Pandey et al., 2020). The use of 3D printing thus enables the production of an oral drug delivery system that allows for

customized formulation with control over size, shape, and release rate (Pandey et al., 2020). Additionally, 3D printing enables us to create internal structures and designs that would be challenging or perhaps impossible to create using more conventional manufacturing techniques (Ma et al., 2022; Pandey et al., 2020; Pitzanti et al., 2022; Sadia et al., 2018). Researchers have recently attempted to apply 3D printing technologies for manufacturing tablets for colon drug delivery (Almeida et al., 2021; Charbe et al., 2017; Mirdamadian et al., 2022). However, there is still a critical need for a drug delivery system that can solely target the colon's inflammatory tissue. A mechanism like this could increase the anti-inflammatory drug's therapeutic effectiveness and minimize its systemic negative effects (Makhlof et al., 2009).

In recent years, several strategies for colon-targeted drug delivery have been proposed, taking into account the physiological properties of the colon (Moutaharrik et al., 2021), based on which time-based, enzymatically degradable, and pH-responsive drug delivery systems were developed. The majority of colonic drug delivery systems used to treat IBD that are currently available on the market are made of pH-responsive polymers that take advantage of pH changes in the gastrointestinal tract (Awad et al., 2022; Bukhovets et al., 2020; Goyanes, Chang, et al.,
2015; Moutaharrik et al., 2021). For the production of pH-responsive oral drug delivery systems, Eudragit® series polymethacrylates from Evonik Röhm GmbH are frequently utilized. A unique methyl acrylate-methyl methacrylate-methacrylic acid terpolymer called Eudragit® FS100, hereinafter referred to as EURFS100, dissolves at pH levels higher than 7 due to the free carboxylic acid moiety on the polymer chain, which makes it a suitable candidate for colon drug administration (Balogh et al., 2017; Bukhovets et al., 2020). The most popular manufacturing method for creating pH-responsive colonic medication delivery devices using pH-responsive polymers is the coating of dosage forms. This method has numerous limitations; for instance, concerns for the environment and human health are raised often due to the use of organic solvents in the coating process. Another drawback of film-coated dosage forms is dose dumping due to defects in the film coating (Zhang, 2016). Finally, the coating does not provide a sustained drug release profile since the drug release initiates upon dissolving the coated layer (Makhlof et al., 2009). Therefore, 3D printing of pH-responsive polymers can address the limitation of current manufacturing methods.

Another major limitation of traditional tablets and powder-based capsules designed for colonic distribution is their frequently insufficient disintegration and dissolution due to the low fluid level in the colon (Awad et al., 2022; Charbe et al., 2017; Tannergren et al., 2009). Therefore, it would be advantageous if we could provide the medication as a liquid and protect the drug from the harsh acidic environment of the stomach or the proteolytic activity of the enzymes in the small intestine; for instance, in the form of liquid-filled hard capsules or tablets (Charbe et al., 2017). Using this approach, the inflamed mucosal surfaces can be targeted by (bio)therapeutics employing hydrogels as delivery methods (Aprodu et al., 2019; Tate et al., 2001). The aim of this study is to employ a mucoadhesive or thermo-responsive hydrogel in combination with 3D printing technology to manufacture 3D printed tablets that can contain the hydrogel for targeted colonic oral drug delivery application. A thermo-responsive hydrogel was employed due to its preparation practicality and feasibility in its sole state as by gelling at various polymer concentrations at 37°C, not only controlled drug release can be achieved but also the gel will maintain its state throughout the entire GI tract, where the temperature is usually 37°C. Methylcellulose (MC) hydrogel, a member of the cellulose ether family, was selected as a suitable candidate for the local administration of pharmaceuticals given the benefits of minimizing systemic exposure to such treatments and biocompatibility.

In this study, GlcNAc was incorporated into MC hydrogel after which the hydrogel was filled in a 3D printed biodegradable and pH-responsive shell made of a blend of EURFS100 and polylactic acid (PLA) polymers. PLA as a biodegradable polymer tremendously used in the biomedical field was used in the 3D printing process to overcome the limitations of EURFS100's printability; this improvement was due to PLA's good processability, low processing temperature (130 ºC), and stability up to 200 ºC (DeStefano et al., 2020; Kontárová et al., 2020; Ramot et al., 2016; Vert, 2015). The primary reason for incorporating GlcNAc into a hydrogel and the core-shell structure of the tablet was to prevent the rapid drug release in the upper GI tract while enhancing its dissolution in the dry colon environment. Furthermore, it is important to note that directly mixing GlcNAc into the 3D printed shell could lead to the thermal decomposition of GlcNAc due to the high processing temperature involved. As a result, this manufacturing approach not only addresses the immediate drug release issue but also opens doors for potential future combination therapies that involve thermosensitive drugs. Various ratios of EURFS100 and PLA, different concentrations of MC hydrogel, and different printing designs in terms of infill and discharge were investigated to optimize the printed tablets. Rheological properties of polymers and hydrogels were studied, and the EURFS100 and PLA polymers were characterized in terms of thermal properties. Scanning electron microscopy (SEM) was carried out to evaluate the physical properties of the tablets. Moreover, the effects of MC hydrogel concentration and EURFS100 and PLA polymer ratio on drug release patterns and kinetics were assessed. Ultimately, all components of the tablet including 3D printed shells, hydrogels, and various concentrations of GlcNAc were assessed in terms of cytotoxicity.

## 2.1. Materials

GlcNAc, dithiothreitol, $(NH_4)Fe(SO_4)_2 \cdot 12H_2O$, sodium hydroxide (NaOH), and sulfamic acid was purchased from Carl Roth (Germany). Eudragit® FS100 polymer was kindly gifted from Evonik (Germany). Luminy® PLA LX930 was purchased from Total Corbion PLA (Thailand) Ltd. MC was purchased from Sigma–Aldrich (Germany) and used as a hydrogel structure. Hydrochloric acid (37%), and Phosphate buffered saline (PBS) tablets were purchased from VWR Chemicals, LLC (USA) and Thermo Fisher Scientific (USA), respectively. Dialysis tubing cellulose membrane (molecular weight cut-off=14,000), dimethyl sulfoxide (DMSO), 3-methyl-2-benzothiazolinonhydrazon, and cell proliferation kit II (XTT) were purchased from Sigma–Aldrich (Germany). Polymerase chain reaction (PCR) plates, Gibco™ Dulbecco's modified Eagle's medium (DMEM), and fetal calf serum (FCS) were purchased from Thermo Fisher Scientific (USA). Finally, all materials were used without further purification.

## 2.2. Methods

### 2.2.1. MC hydrogel preparation and drug loading

A previously documented approach for creating MC hydrogels was used in this work; although, it was further modified due to the addition of a thermosensitive drug in the later stages of the study (Altomare et al., 2016; Cochis et al., 2018; Jiang, 2021; Liu & Yao, 2015). Briefly, aqueous solutions were prepared by the addition of 0.1, 0.2, 0.3 and 0.4 g of MC to 10 ml of water to produce 10 ml of 1%, 2%, 3%, and 4% w/v MC hydrogel, respectively. For drug-incorporated hydrogels, a 30 mg/ml GlcNAc solution (10 ml) was made after which 0.1, 0.2, 0,3, and 0.4 g of MC was added to GlcNAc solution on ice to prepare 10 ml of MC 1%, 2%, 3%, and 4% w/v solutions, respectively. The samples were then refrigerated for 3 days to obtain fully transparent and bubble-free hydrogels. Before conducting 3D printing tests, the

gels were freshly prepared. The chemical structure of MC (Figure 1A) and GlcNAc (Figure 1B) are depicted in Figure 1.

2.2.2. Polymer blend preparation

PLA granules were powdered using a pulverisette 14 variable speed rotor mill (Fritsch, Germany), and EURFS100 as a powder was used as received. They were kept in a vacuum oven (Memmert, Germany) at 40 °C for 5 h prior to use. Polymeric blends of EURFS100 with 10%, 20%, 30%, and 40% PLA were prepared by physical mixing of the polymers in a container. The amount of PLA is shown as % of the polymer dry weight. Figures 2A and 2B show the chemical structure of PLA and EURFS100, respectively.

2.2.3. Design and printing of the tablets

Arburg 200-3X 3D printer (Arburg, Germany) shown in Figure 3A was used to print the tablets. The 3D printer has a carrier with three axes of motion and two discharge units. Using this system, components from two materials or more with complex shapes and/or support structures can be fabricated. To produce a precise and homogenous item, the procedure begins with injection molding and ends with extrusion through a nozzle with a needle inside that forces the material out, droplet by droplet. By modifying slicing, droplet size, and process control impacting the layer-by-layer build process, the manufacturing process can be specifically tailored toward particular needs. The optimum processing temperatures for our experiments in the discharge unit, zone 1 and 2, the material feed unit, and the build chamber were 160, 160, 135, 35, and 35 ºC, respectively (Figure 3B).

For the entire process of 3D printing, the optimum values of the nozzle diameter, melt (printing) speed, melt pressure, discharge, dosage stroke, and back pressure were 0.25 mm, 20 mm/s, 700 bar, 80%, 5 mm, and 7 bar, respectively. Each tablet contained three distinct sections, including the top, bottom, and middle chamber. The tablet's diameter and thickness, according to the design, were 12 and 4 mm, respectively. After setting up all printing parameters, printing the tablets was conducted by adding a few grams of the polymer blend to the hopper after which purging and droplet formation were initiated in order to confirm the stability of discharge. The 3D printed tablets were then produced using the design created by SolidWorks software.

Figure 4 depicts the 3D printing process schematically. The graphic shows the three phases involved in 3D printing; the bottom layers and a portion of the middle chamber were initially printed (Figure 4A), followed by the injection of MC hydrogel loaded with GlcNAc (Figure 4B), and then the remaining layers were printed to enclose the tablets (Figure 4C). Prior to printing, the best settings were adjusted by experimenting with droplet formation and discharge rate. The temperatures of various zones were then set up by comparing the melt flow consistency to the melt pressure stability. Table 1 represents the prepared samples along with their labels. All through the article, these labels are used.

To identify the optimal processing parameters of the tablets and achieve the desired drug release kinetics, two main experiments were conducted (Table 2). In the first experiment, the effect of polymer blending ratio on printability, physical properties of the tablets, and drug release was assessed from which the optimum blending ratio was selected for the second experiment. In the second experiment, on the other hand, the effect of MC concentration on the processability, physical characteristics of the tablets and drug release was studied. After printing the tablets, they were assessed in terms of weight using an AUW120D analytical

balance (Shimadzu, Japan), diameter, and thickness using a digital micrometer (Accud, Austria). For each group of experiments, 3 samples were analyzed.

2.2.4. Scanning electron microscopy (SEM)

SEM was carried out using the Phenom Pro G6 Desktop scanning electron microscope (Thermo Fisher Scientific, USA) to study the morphology of the 3D printed shells containing EURFS100/PLA (80/20 and 70/30 w/w). Additionally, 3D printed tablets with the same polymer blending ratios containing GlcNAc-loaded MC hydrogel (2% and 3% w/v) that had been freeze-dried were analyzed using SEM. The samples were sputter-coated with gold under vacuum conditions in a Lnxor $^{Au}$ vacuum in order to be conductible. After that, the samples were placed on a standard sample holder and introduced into the apparatus. The accelerating voltage was 10 kV at various magnifications.

2.2.5. Rheological characterization

All of our rheological studies were carried out on a Discovery Hybrid DHR-1 (TA Instruments, USA) using various plates. Three repeat trials per sample were carried out in each experiment, and each experiment was carried out in two independent batches of hydrogels and polymers.

2.2.5.1. Hydrogel rheology analysis

Two different concentrations of MC hydrogel (2% and 3% w/v) were examined. The MC hydrogels were characterized with the rheometer, equipped with rotational parallel plate (Peltier plate steel) geometry (diameter = 40 mm, working gap = 500 µm). An isolation chamber was applied to the plate to prevent dehydration of the hydrogel under test.

1.2.5.1.1. Frequency sweep tests

Each rheological characterization experiment consisted of frequency sweeps at 1% strain, repeated at 25 and 37 °C. Storage (G′) and loss (G″) moduli were recorded in regard to angular frequency from 0.1 to 248.4 rad/s, with 5 points taken per decade. Samples were stored at 4 °C prior to testing. For frequency sweep tests carried out at 25 and 37 °C, samples were allowed to equilibrate for 30 min prior to testing, with the Peltier stage set to each of them (Law et al., 2018).

2.2.5.1.2. Flow ramp tests

Another method was used at two distinct temperatures of 25 and 37 °C to examine the potential changes in hydrogel behavior with various concentrations at two different temperatures. The shear rate was increased from 1 to 250 $s^{-1}$ in order to investigate the hydrogel viscosity.

2.2.5.2. Polymer rheology experiment

To determine the characteristics of the polymers and their mixture in response to time, temperature, and angular frequency, the rheometer equipped with parallel plates, ETC Steel (diameter = 25 mm, working gap = 500 µm) was used to analyze the samples. Rheology measurements were carried out to examine the viscoelastic behavior of EURFS 100 alone and in combination with PLA at the melted state to investigate the alteration of the elastic

modulus (G') and plastic modulus (G″), according to frequency sweep experiments. To check for stability, samples were heated up to 160 °C mimicking the printing temperature.

2.2.6. Thermal gravimetric analysis (TGA)

To understand the thermal stability of the polymers and the impact of the processing temperature of 3D printing on the degradation of polymers, TGA was performed on all the polymers used in 3D printing utilizing TA Q500 thermogravimetric equipment (TA Instruments, USA). Under nitrogen purge (50 ml/min), vacuum-dried samples were heated at a rate of 10°C/min from 25 to 700 °C. The data was then analyzed using TA 2000 analysis software.

2.2.7. Differential Scanning Calorimetry (DSC)

As different blends of polymers were utilized, the thermal transition of the polymers was analyzed using DSC Q2000 equipment (TA Instruments, USA). The weight of samples was 5 mg. Crystallinity and melting point values were determined by analyzing the DSC curves. The value acquired from the TGA would indicate the maximum temperature set for the DSC for each sample trial because the DSC equipment can only endure temperatures that result in a 1% weight loss. The samples were examined by starting at 25 °C and increasing the temperature at a rate of 10 °C/min until 200 °C was reached. There were two full cycles of heating and cooling to get the intended values. The second heating and cooling cycles were examined using the same TA universal method used in TGA.

2.2.8. Dissolution testing of printed tablets and drug assay

2.2.8.1. Dissolution study

The dissolution studies, carried out under physiologically relevant conditions, were the primary criterion for determining if the 3D printed tablets were capable of releasing the drug in the colon and withstanding the acidic condition of the upper gastrointestinal tract. For 2 h, samples were placed in HCl 0.1 M simulating the stomach fluid having a pH of 1-2, followed by 3 h in PBS with pH 6.8 simulating the small intestine, and 24 h in PBS with pH 7.4 simulating the colon. These buffer systems were chosen in accordance with the pH changes in the gastrointestinal tract from the stomach (pH 1.5) and proximal small intestine (pH 6.0-6.8) to the ileocecal area (pH 7.3) (Makhlof et al., 2009). Each sample was suspended in 50 ml of the release medium and incubated in a shaker (Infors HT Ecotron, Switzerland) at 37 ºC ± 0.5 and 100 rpm. There were three samples in each group. Samples were then withdrawn at specific interval times of 1, 2, 3, 4, 5, 6, 7, 8, 9, 10, 11, 12, 13, 22, 23, 24, 25, 26, 27, 28, and 29 h. After predetermined time intervals, 500 µl samples were collected and analyzed. To keep the volume extent, a precise amount of fresh medium (500 µl) was supplied after each sampling. The results were then presented as a cumulative percentage of GlcNAc released at each examined time.

2.2.8.2. GlcNAc assay

The 3-methyl-2-benzothiazolinone hydrazone (MBTH) assay was used to determine the drug concentration in the samples since the absorbance stays consistent per reducing end regardless of the length of the chito-oligosaccharide. Hetero-chitooligosaccharides are mixtures of multiple oligomers, whereas homo-chitooligosaccharides are oligomers made exclusively of either GlcN or GlcNAc units. To our knowledge, the MBTH approach, which

can detect concentrations as low as 5 µM, is the most sensitive reducing end test for the detection of chito-oligosaccharides (Horn & Eijsink, 2004; Tabassum et al., 2021). The 3D printed shells and tablets containing the drug-free hydrogel were examined; the drug-free hydrogels were assessed to ensure that the hydrogel itself did not impact the final drug release data. The percentage of the released drug was determined by loading 40 µl of the dissolution test samples into PCR plates, mixing them with 40 µl of 0.5 M NaOH, and then adding 40 µl of a solution containing 1.5 mg/ml 3-methyl-2-benzothiazolinonhydrazon and 0.75 mg/ml dithiothreitol. The resulting solutions were then completely mixed with 80 µl of 0.5 % (w/v) $(NH_4)Fe(SO_4)_2 \cdot 12H_2O$ , 0.5% (w/v) sulfamic acid, and 0.25 M HCl after being incubated at 80 °C for 15 min. Samples were cooled down to room temperature and absorption was measured at 620 nm (Schmitz, 2021). The assay was performed in triplicate and sink conditions were met throughout the dissolution test. For each measuring cycle, a freshly prepared GlcNAc calibration curve was created.

2.2.9. Drug release kinetics

Higuchi, Korsmeyer-Peppas, and Peppas-Sahlin were selected as the mathematical models to fit the experimental data obtained from the drug release measurements from the 3D printed tablets.

2.2.9.1. Higuchi model

The Higuchi model is represented by the following equation:

$$\frac{M_t}{M_\infty} = kt^{0.5}$$

Eq.(1)

Where $M_t$ represents the cumulative drug release at time point t, $M_\infty$ denotes the cumulative drug release over an infinitely extended period, and $k$ represents the kinetic constants specific to the drug/polymer system (Linares et al., 2019).

2.2.9.2. Korsmeyer-Peppas model

The power-law model, also known as the Korsmeyer-Peppas model, is the most common kinetic model in the studies of drug release, showing an exponential relationship between time and drug release. This model is used to describe the non-Fickian drug release from a polymeric structure (Algahtani et al., 2020; Heredia et al., 2022). The Korsmeyer-Peppas model is represented by the following equation:

$$\frac{M_t}{M_\infty} = kt^n$$

Eq.(2)

Where $M_t$ and $M_\infty$ are the absolute cumulative amount of drug released at time t and infinite time, respectively. The release kinetic constant (k) accounts for the system's structural and geometrical properties, whereas the release exponent (n) reveals the drug release process (Siepmann & Peppas, 2012). In reality, Eq. (2) provides two unique and plausible explanations for the two specific circumstances of n=0.5 (showing drug release regulated by diffusion) and n =1.0 (indicating that the drug release is controlled by swelling). The combination of both phenomena can be determined by values of n between 0.5 and 1.0 (anomalous transport). It must be noted that the two extreme values of the exponent n, 0.5

and 1.0, are exclusively applicable to slab geometry. Table 3 displays the n value associated with each geometry. Polymer scientists refer to the mechanism that generates the zero-order release for slabs as case-II transport. The rate-controlling phase in this process is the relaxation of the macromolecules that happens when water is infused into the system. Water works as a plasticizer and lowers the polymer's glass transition temperature (Siepmann & Peppas, 2012; Windolf et al., 2021).

2.2.9.3. Peppas-Sahlin model

This model is expressed by the following equation:

$$\frac{M_t}{M_\infty} = k_d t^m + k_r t^{2m} \quad \text{Eq.(3)}$$

where the Fickian contribution constitutes the first term ($k_d t^m$) and the Case-II relaxational contribution is the second term ($k_r t^{2m}$). The coefficient $m$ is the purely Fickian diffusion exponent for a device with controlled release of varying geometrical shapes (Peppas & Sahlin, 1989). The Peppas-Sahlin model is defined based on the assumption that the release mechanism is governed by two processes: diffusion and polymer relaxation. This model contains three parameters, where the diffusional contribution represented by constant $k_d$and the relaxational contribution represented by constant $k_r$ were calculated based on the quadratic regression (Linares et al., 2019). Additionally, the shape parameter, represented by $m$ was calculated according to the dimensions of tablets for each condition (Peppas & Sahlin, 1989; Pereira et al., 2023). The following equation was used to calculate the percentage of drug release through Fickian mechanism (F):

$$\mathrm{F} = \frac{1}{1 + \frac{k_d}{k_r} t^m}$$

Eq.(4)

While the ratio of relaxational (R) over Fickian (F) mechanism was obtained according to the following equation:

$$\frac{R}{F} = \frac{k_r}{k_d} t^m \quad \text{Eq.(5)}$$

When $\frac{R}{F} = 1$, the release mechanism contains both erosion and diffusion equally. If $\frac{R}{F} > 1$, the relaxation (erosion) dominates, while for $\frac{R}{F} > 1$, diffusion dominates (Peppas & Sahlin, 1989; Unagolla & Jayasuriya, 2018).

The first 60% of cumulative drug release data were taken into account in the Korsmeyer-Peppas model to determine the mechanism of drug release (Ahuja et al., 2007; Ritger & Peppas, 1987; Rostamitabar et al., 2021; Unagolla & Jayasuriya, 2018). Data from in vitro drug release studies were plotted as log cumulative percentage drug release versus log time to evaluate the release kinetics. Finally, the mean dissolution time (MDT), as the sum of the various release fraction periods during the dissolution studies divided by the initial loading dose, was also calculated (Talukder & Fassihi, 2008; Vemula & Veerareddy, 2013) using the following equation:

$MDT = \sum_{i=1}^{n} \widehat{t_i} \frac{M_t}{M_\infty}$

Eq.(6)

Where $M_t$ and $M_\infty$ are the fraction of dose released in time $\widehat{t_i} = (t_i + t_{i-1})/2$ and the total amount of drug released. To understand the colon-specific release from tablets, T10% and T80% (duration in hours to take 10% and 80% drug release, respectively) were also computed.

2.2.10. *In vitro* cell viability studies

Mouse fibroblasts cells (L929) were cultured at 37 °C and 5% CO2 in DMEM with 10% FCS. Cells at passage 4 were used for the viability experiments using XTT. The 3D printed shell samples and MC powder were sterilized by ethylene oxide, while the drug solution was sterilized using a 0.22 µm syringe filter prior to the tests. To test the cytotoxicity of the polymer blends, 3D printed shells comprising 20% and 30 % PLA in combination with EURFS 100 were produced. The same shells that contained MC hydrogel (0.3% w/v) were also included. Separate solutions were made to test the cytotoxicity of various concentrations of MC (0.1%, 0.05 %, and 0.025% w/v) and GlcNAc (0.3, 0.15, 0.075, and 0.0375 mg/ml). The samples were all sterilized and tested. XTT assay was performed according to the ISO 10993-12. In short, samples, positive control, and negative control were incubated in the DMEM culture medium for 24 h. The negative control was DMEM, and the positive control was DMSO. Cells were seeded in 96-well plates ($1 \times 10^4$ cells per well) and were allowed to adhere to the wells for 24 h. After 24 h, the medium of the well-plates was exchanged with that of the samples, positive control, and negative control or blank. After an incubation period of one day, the XTT assay was performed according to the manufacturer's protocol. The absorbance was measured in a multimode microplate reader M200 (Tecan, Switzerland) at 450 nm with a reference wavelength of 650 nm. The assessment was performed for three replicates.

2.2.11. Statistical analysis

All data are presented as mean ± standard deviation. To determine the statistical difference between the weight, thickness, diameter, and drug content of the samples, two-way ANOVA, followed by Tukey's multiple comparison post hoc test, was performed. Furthermore, one-way ANOVA, followed by Tukey's test, was used to assess the differences between the XTT data. Origin 2019 (OriginLab, USA) was used to conduct the statistical analysis, and a *p*-value <0.05 was considered significant.

3. Results and discussion

3.1. Design and printing

The printing method included simultaneous optimization for the three polymer blends and several 3D printing settings, including discharge rate, layer height, and consequently droplet size, to guarantee the printability of the polymers. In this step, the printing process was continuously monitored, taking into account the melt flow consistency, discharge rate, and melt pressure. Table 4 shows all of the polymer blends used for processing optimization. Amongst the three polymer blends of 60/40, 70/30, and 80/20 w/w EURFS100 to PLA, 80/20 w/w EURFS100 to PLA showed the most stable printing and consistent production. The printing setting initially appeared to be steady when using a PLA ratio of 30%, but

throughout the process, a number of irregularities and pressure shifts occurred. Therefore, it was concluded to proceed with 20% and 30% PLA in order to examine further properties of the tablets, particularly drug release kinetics. It should be added that when the PLA ratio went down to 10% printability was not improved and when it went up to 40%, the polymers dissociation in printing happened.

The discharge rate of 80 % and the resulting 400 μm layer height was selected as optimum parameters for the stable printing of the tablets (Figure 5A). Based on this setting, a total of 10 layers were printed, 2 layers at the top and bottom and 6 layers in the middle, to reach the theoretical tablet thickness. The top, bottom, and middle sections were evaluated with two different infill percentages (Table 5). The middle portion's infill percentage was set at 20% and 40%, while the top and bottom layers' infill percentages were chosen at 60% and 80%. According to the printing outcomes, there was not enough room for the hydrogel to be injected when the infill of the middle section reached 40%; therefore, the hydrogel remained on top of the layer. A 60% infill was tested for the top and bottom layers, but there was a significant amount of hydrogel leakage. Therefore, the infill of 20% for the middle section and 80% for the top and bottom was selected as the final setting for printing the tablets (Figure 5B).

3.2. Physical characteristics of the tablets

Figure 6 depicts all of the 3D printed samples' physical examinations, including an image of three 3D printed tablets. MC 1% and MC 4% w/v were not included in the trials since the gels had significantly low or high viscosity, respectively, making it impossible to conduct the trials. Moreover, printing did not proceed with 10% and 40% PLA. For PLA 10%, no improvement in the printing was seen, while for the PLA 40%, the polymer dissociation in printing happened. Regarding the weight of the tablets (Figure 6B), no statistical difference was observed between samples with different polymer blending ratios or MC concentrations. MC 2 % w/v hydrogel-filled tablets showed average thicknesses higher than the theoretical value of 4 mm (Figure 6C); this could be due to the less viscous structure of MC 2% w/v compare to MC 3% w/v hydrogel. While printing, the size seemed to be normal, but after a few hours, the dimensions changed as a result of water diffusion through various layers, which caused the polymers to swell or even changed the structure of the polymers (Banjo et al., 2022; Lenz et al., 2021) . The data also shows that the thicknesses of the tablets containing MC 2 % w/v hydrogel were significantly higher than those with MC 3 % w/v hydrogel. Finally, it was demonstrated that compared to the tablets containing MC 3% w/v hydrogel, the diameter of the tablets containing MC 2% w/v was significantly lower and that the average diameter of the samples with MC 2% w/v was lower than the theoretical value of 12 mm (Figure 6D).

3.2.1. SEM analysis

SEM images show the surface morphology of the 3D printed tablets (Figure 7), displaying smooth, compact, and occasionally uneven structures due to the layers' merging. A whole view of the tablet was also shown (Figure 7A). The images also showed evidence of slight surface roughness at certain spots of the samples (Figures 7B and 7C). This could be due to the low extrusion temperature, which led to the incomplete melting of the polymers, leading to slight uneven surface of the finished product (Lamichhane et al., 2019). Based on the SEM images, there was no significant difference between samples with different polymers blending ratios or MC hydrogel concentrations.

3.3. Rheological analysis

3.3.1. Rheology of the hydrogels

The rheology of the hydrogel, impacted by the concentration of MC, is crucial in the manufacturing of the tablets to ensure that the hydrogel can be injected with precision. Figure 6 on a log−log scale provides an illustration of the MC 3% and 2% w/v hydrogels' rheology data. In order to examine the behavior of the hydrogels, due to the thermosensitive characteristics of MC hydrogels, the temperatures of 25 and 37 °C were chosen since the tablets were produced at room temperature and then examined at body temperature for drug release investigations (Aprodu et al., 2019; Huang et al., 2020). Figure 6 provides an illustration of the MC 3% and 2% w/v hydrogels' rheology data. Both hydrogels showed close values for G' and G" across the low angular frequency ramp (Figure 8A), showing stable hydrogel behavior. Moreover, MC 3 % showed more thermo-responsive behavior since both G' and G" were higher at 37 compared to 25 °C. MC 3% and 2% w/v hydrogels also showed close values in terms of viscosity by increasing the shear rate at 37 and 25 °C. By increasing the shear rate, the viscosity of all samples decreased (Figure 8B), demonstrating shear thinning properties of the samples (Negim et al., 2014; Wilkes, 1981).

3.3.2. Rheology of the polymers

Thermal stability is crucial when processing a novel polymer utilizing melting techniques. Since the polymers are utilized in 3D printing, conventional viscoelastic analysis using frequency scans is not appropriate for a complete investigation of the behavior of the materials. A straightforward testing approach was employed in this study based on a time sequence of frequency scans in order to obtain the viscoelastic moduli's basic frequency dependency (Filippone et al., 2015). The kinetics of the degrading phenomenon was our major consideration once the polymer's initial qualities were established. The objective was to measure the moduli as a function of time in order to track the progression. Figure 9 on a log-linear scale depicts the G' and G" changes of the polymer blends of EURFS100/PLA (80/20 and 70/30 w/w) and pure EURFS100 and PLA versus time at various angular frequencies at 160 °C. Due to the impact of degradation on the dynamics of small fractions of the polymer chain, the viscoelastic moduli of EURFS100 (Figure 9A) exhibited a slight increase over time, with larger changes at lower frequencies. The described phenomenon of heated EURFS 100 implies that a cross-linked rubberlike molecular structure may be formed at elevated temperatures which may also affect drug release (Balogh et al., 2017). It is clear from PLA behavior (Figure 9B) that at higher frequencies, there were less differences between G' and G" values than at lower frequencies. At lower frequencies, however, G" is dominating G', although similar changes are barely noticeable for the other samples, especially for EURFS100. According to Figure 9B, PLA showed time-independent characteristics under a certain angular frequency (Lenz et al., 2021; Wilkes, 1981). The changes in the viscoelastic moduli at the start of the procedure were considerably more visible by increasing the PLA blending ratio (Figures 9C and 9D). In comparison to pure EURFS100, its blend with PLA (30% w/w) (Figure 9D) at lower frequencies has demonstrated higher rise in the viscoelastic moduli.

3.4. TGA analysis

Finding the processing temperature range is essential to prevent degradation and other undesired chemical changes while 3D printing the polymer blend since the heating process is the first step in creating the polymeric structure of tablets. To understand the thermal stability

of the polymers and the impact of the processing temperature of 3D printing on the degradation of polymers, TGA was done. According to TGA curves illustrated in Figure 10A, no weight loss was detected from 0 to ~180 ºC for all samples. TGA analysis showed that all polymer blends had a weight loss stage between 180 and 200 ºC, albeit each had a distinct slope in terms of weight loss, showing poorer thermal stabilities of the blends with more PLA. The step from 180 to 200 ºC in the mass loss was due to the evaporation of some volatiles in the structure (Balogh et al., 2017). The decomposition stage was found in the range of 250-300 ºC for PLA, 300-400 ºC for EURFS100, 350-380 ºC for EURFS100/PLA (80/20 w/w), and 300-380 ºC for 70/30 w/w EURFS100/PLA, indicating lower thermal stabilities of pure PLA and EURFS100. The decomposition of the mixture of EURFS100 and PLA (80/20 w/w), as shown in the TGA graph (Figure 10A), initiated at a higher temperature (350 ºC) compared to other samples, showed the higher thermal stability of these samples among others. The differential thermal analysis (DTA) curves shown in (Figure 10B) imply that the polymer blend EURFS100/PLA (80/20 w/w) exhibited a slower rate of degradation compared to other samples; however, the decomposition range was broader.

### 3.5. DSC analysis

The temperature at which 1 % weight loss happened was below 200 ºC for all samples; thus, this temperature was set for further DSC analysis. The DSC data was divided into two graphs, one for the heating cycle and the other for the cooling cycle (Figure 11). The highest resemblance in terms of thermal behavior between the heating and cooling of EURFS100 and its blend with PLA (20% w/w) was observed using the DSC graph analysis. This blend's resemblance to the target polymer may hold great promise for 3D printing such that similar characteristics of the polymer of interest, EURFS100 in this case, are maintained while improving the processability. PLA (20% w/w) had the best stability and consistency while 3D printing, as proven by the performed analyses. Amorphous EURFS100 and PLA both demonstrated Tg at about 55 and 60 °C, respectively (Figures 11A and 11B). The melting-like glass transition of EURFS100 is analogous to the thermal behavior of other amorphous Eudragit polymers, such as Eudragit E (Balogh et al., 2017). Due to the multiple Tg of the polymers, the Tg-related peak for the polymer blends occurs at two distinct temperatures. Another peak was observed in the polymer blends and EURFS100 beginning at 170 °C with a mild baseline shift. This shift can be attributed to a number of factors, including the vaporization of a volatile compound (such as even bound water), as also shown by thermogravimetric TGA measurements (Figure 8), or the presumed molecular changes at higher temperatures, as seen by the rheology measurements, but it is not at the actual glass transition (Balogh et al., 2017).

### 3.6. Drug release and kinetic models

The first and most important analysis that should be performed on the tablets is the drug release experiments under physiologically relevant circumstances. Figure 12A displays the cumulative release profile of four distinct circumstances. After the release experiment was performed, each tablet was subjected to vigorous shaking and ultrasonication in order to ensure that the full amount of drug incorporated into the construct was released in the medium so that the total amount of incorporated drug can be calculated (Figure 12B). The results showed that throughout the 2 h at pH 1.2, no drug was released from the tablets. The polymer began to dissolve when the medium was with that of pH 6.8, allowing the diffusion and release of the drug (Figure 12A). Based on the differences in pH between the three

organs, the main goal of the research was to have a form of controlled drug release over the colon while retaining the least amount of drug released over the stomach and small intestine.

According to the physical characterization of the 3D printed tablets prior to release experiments and the drug release data, the tablets prepared by the polymer blend of EURFS100/PLA (80/20 w/w) in combination with drug-loaded MC 3% w/v hydrogel showed the best-sustained drug release profile (Figure 12A). This group also showed a limited amount of drug release in the media that resembled the stomach and small intestine (less than 20 % overall) amongst other groups, which was the ultimate goal of this study, and more than 90 % of the drug was released within 29 h. However, samples with MC 2% w/v were considerably better for manually injecting the hydrogel and having the correct drug contents but showed leakages (Figure12B). Moreover, due to the rapid infiltration of hydrogel into the 3D printed constructs, the tablets started to distort due to the hydrolytic breakdown of PLA caused by breaking the ester linkages as a result of the diffusion of water molecules, which ultimately impacted the dimensions of the tablets (Banjo et al., 2022). The drug-free tablets and the shells both behaved similar to the blank samples and did not interfere with the detection of GlcNAc.

One of the key benefits of the 3D printing design of the tablets was that the regulated drug release could take place due to the gradual degradation of the structure without taking pH sensitivity of the polymer into account. However, when EURFS100 is used for coating the tablet, the drug release occurs promptly upon reaching the colon pH value. It was observed that the tablets stayed integrated until the completion of the drug release studies although lost rigidity (Figure 12C); this could play a role in the sustained drug release profile. The drug release data showed comparable results to those observed with previous Eudragit compression-coated or solvent-coated tablets (Goyanes et al., 2015; Veerareddy & Vemula, 2012; Vemula, 2015a, 2015b).

The drug release in non-Fickian diffusion can be influenced by a number of factors and mathematical models, including the first-order release kinetics model, the Higuchi release kinetics model, the Korsmeyer-Peppas release kinetics model, and Peppas-Sahlin model (Algahtani et al., 2020). Higuchi, Korsmeyer-Peppas, and Peppas-Sahlin release kinetic models were used to describe the non-Fickian drug release kinetics from a polymeric structure. Korsmeyer-Peppas model is useful when the release mechanism is unknown or when there are multiple drug release phenomena (Algahtani et al., 2020; Heredia et al., 2022). The general solute-release behavior of controlled-release polymeric devices is described by this model (Ritger & Peppas, 1987). Since the rate of erosion of the tablets in the dissolution media varied with regard to pH values, it was decided to take the release data related to the third medium (PBS pH 7.4) as the target medium rather than all the media due to pH variations. The kinetic contact parameters k and $R^2$ values related to the Higuchi model are provided in Table 6 for all samples. The results showed that tablets containing higher amount of EURFS100 polymer had higher $R^2$ values, indicating that the Fickian diffusion mechanism was more pronounced in those samples. However, the $R^2$ is not close to 1 in this model, which shows the drug release was not primarily controlled by diffusion.

According to Korsmeyer-Peppas model, the underlying drug release mechanism is described by the diffusional constant n, and the release behavior can be classified into Fickian diffusion, anomalous transport, or case-II transport depending on the value of n (Algahtani et al., 2020; Windolf et al., 2021). For 3D printed samples with 80% w/w EURFS100 containing GlcNAc loaded hydrogels of 3 % w/v and 2 % w/v MC, exponent n values of 0.8425 and 0.6641 were obtained, respectively. This indicates anomalous drug transport from

the swellable matrices. With regard to values of n, it can be concluded that diffusion and swelling processes influenced the release mechanism of samples containing EURFS100/PLA (80/20 w/w). There were differences between the value of n in two distinct MC concentrations for PLA 20% which is the effect of a higher swelling ratio for higher concentrated hydrogel (MC 3%).

The increased use of hydrogels in drug delivery system formulations is based on their capacity to form a hydrogel network when swollen, which traps the drug and serves as a barrier to its release to the medium (Carbinatto et al., 2014). Hydrogels are hydrophilic polymers that absorb large quantities of water. In this regard, the hydrogels' ability to swell is a critical attribute that should influence the rate at which drugs are released by regulating the penetrant's rate of diffusion into the matrix as well as the drug's dissolution and diffusion across the hydrogel layer of the swelled matrix (Carbinatto et al., 2014). The model could make a good fit to the drug release data when the regression coefficient, $R^2$, was close to 1 (Wójcik-Pastuszka et al., 2019). Given the system's characteristics, it appeared that the Korsmeyer-Peppas model could be a reliable model for describing the mass transfer in this system. Based on the information in Table 7, since $R^2$ was more than 0.9 for all samples, and experimental data presented in the study, Korsmeyer-Peppas model could reasonably explain the release behavior in spite of the fact the model is unable to predict the mass transport mechanism for the samples with higher PLA content (30% w/w) as well as the importance of each mechanism.

According to the parameters from Table 8 in the Peppas-Sahlin model, it became evident that the model predominantly showed the relaxation or erosion of polymer chains as the primary mechanism for drug release. This is evident from the higher values associated with the relaxation constant compared to the diffusional constant. However, it should be noted that during the initial stages of drug release from the tablets, Fickian diffusion played a controlling mechanism, as indicated by the R/F values falling below 1 (Figure 13). Increasing R/F ratio values with time as shown in Figure 13 indicated an increasing relaxational contribution (Colpo et al., 2018; Peppas & Sahlin, 1989; Pereira et al., 2023; Unagolla & Jayasuriya, 2018). Additionally, the results revealed that a higher content of EURFS100 resulted in higher values of $k_r$ showing that the relaxation of polymer chains was more effective in those tablets compared to the tablets with lower EURFS100 content. Furthermore, the diffusion component exhibited significantly lower values compared to the relaxation of polymer chains, highlighting the dominant role of polymer relaxation in controlling drug release (Bayer, 2023; Colpo et al., 2018; Farrag et al., 2018; Ferrero et al., 2000; Pereira et al., 2023). The above statement was further confirmed by calculating the ratios of relaxation to diffusional contributions (R/F) value, where R/F>1 indicates that the relaxational contribution was predominant over the diffusional contribution (Colpo et al., 2018; Pereira et al., 2023).

Ultimately, in addition to MDT, T10% and T80% (duration in hours to take 10% and 80% drug release, respectively) are shown in Table 9. It is evident that a larger PLA content caused MDT, T10%, and T80% values to increase.

### 3.7. Cytotoxicity analysis

The XTT experiment was carried out to confirm the cytotoxicity of the 3D printed tablets (Figure 14A). After one day of cell culture, the cell viability in the 3D printed samples (Figure 14B) and various concentrations of MC hydrogels (Figure 14C) and drug solutions (Figure 14D) showed no cytotoxicity. The proliferation over days was not examined because

the experiment was conducted to ensure that the tablets, hydrogels, and medication solutions were not toxic to the cells. The findings indicated that the samples were not toxic to the cells and that the drug-loaded hydrogels are promising candidates for further investigation to expand all possibilities of colon drug delivery applications.

## 4. Conclusion and future perspectives

Through this study, a colon-targeting oral drug delivery system based on drug-loaded MC hydrogel and 3D printed polymers was created and optimized. A one-step 3D printing process was employed to produce the pH-responsive polymer framework and encapsulate the medication. Successful encapsulation of GlcNAc into MC hydrogel and protection from the acidic environment of the GIT before reaching the colonic site was done using Eudragit FS100, which prevented early drug release. Although there was a considerable variation between the two polymer blending ratios in the drug release pattern, a smaller amount of PLA demonstrated significantly better-regulated drug release as well as more reproducible printing. This ratio was selected as the optimum candidate for printing the tablets based on the practical 3D printing experiment combined with the polymer blend characterizations including TGA, DSC, and rheology assessment. It was also shown that the cumulative drug release over time was significantly lower when using higher PLA content. Moreover, a higher concentration of MC hydrogel showed a better control over drug release and gelation behavior. According to the Korsmeyer-Peppas kinetic model, both swelling and diffusion had an impact on the drug release mechanism. The Peppas-Sahlin model was able to accurately fit all the data with high $R^2$ values, suggesting that the primary mechanism governing drug release during the experiment is the relaxation of polymer chains. However, because the hydrogel was manually injected, there were certain restrictions with the increased concentration. Overall, the design of pH-responsive 3D printed tablets containing a drug-loaded hydrogel shows promise as a novel oral delivery strategy for improved IBD treatment. In the future studies, the inkjet printing method should be used to automatically inject the drug-loaded hydrogel in the middle of the printing process so that the appropriate drug mixtures and suitable excipients (known as ink) are deposited as small drops in a layer-wise manner on a particular surface (Vaz & Kumar, 2021). The printing process would be considerably more suited to scaling up in general while allowing for more customizability. Our future research will concentrate on evaluating the drug released from hydrogel on disease pathology *in vitro* and *in vivo*, both alone and in combination with other drugs.

## References

Ahuja, N., Katare, O. P., & Singh, B. (2007). Studies on dissolution enhancement and mathematical modeling of drug release of a poorly water-soluble drug using water-soluble carriers. *European Journal of Pharmaceutics and Biopharmaceutics*, *65*(1), 26–38. https://doi.org/10.1016/j.ejpb.2006.07.007

Algahtani, M. S., Mohammed, A. A., Ahmad, J., & Saleh, E. (2020). Development of a 3D printed coating shell to control the drug release of encapsulated immediate-release tablets. *Polymers*, *12*(6). https://doi.org/10.3390/polym12061395

Almeida, A., Linares, V., Mora-Castaño, G., Casas, M., Caraballo, I., & Sarmento, B. (2021). 3D printed systems for colon-specific delivery of camptothecin-loaded chitosan micelles. *European Journal of Pharmaceutics and Biopharmaceutics*, *167*, 48–56. https://doi.org/10.1016/j.ejpb.2021.07.005

Altomare, L., Cochis, A., Carletta, A., Rimondini, L., & Farè, S. (2016). Thermo-responsive methylcellulose hydrogels as temporary substrate for cell sheet biofabrication. Journal of Materials Science: Materials in Medicine, 27(5). https://doi.org/10.1007/s10856-016-5703-8
Aprodu, A., Mantaj, J., Raimi-Abraham, B., & Vllasaliu, D. (2019). Evaluation of a methylcellulose and hyaluronic acid hydrogel as a vehicle for rectal delivery of biologics. *Pharmaceutics*, *11*(3). https://doi.org/10.3390/pharmaceutics11030127
Awad, A., Madla, C. M., McCoubrey, L. E., Ferraro, F., Gavins, F. K. H., Buanz, A., Gaisford, S., Orlu, M., Siepmann, F., Siepmann, J., & Basit, A. W. (2022). Clinical translation of advanced colonic drug delivery technologies. In *Advanced Drug Delivery Reviews* (Vol. 181). Elsevier B.V. https://doi.org/10.1016/j.addr.2021.114076
Balogh, A., Farkas, B., Domokos, A., Farkas, A., Démuth, B., Borbás, E., Nagy, B., Marosi, G., & Nagy, Z. K. (2017). Controlled-release solid dispersions of Eudragit® FS 100 and poorly soluble spironolactone prepared by electrospinning and melt extrusion. *European Polymer Journal*, *95*, 406–417. https://doi.org/10.1016/j.eurpolymj.2017.08.032
Banjo, A. D., Agrawal, V., Auad, M. L., & Celestine, A. D. N. (2022). Moisture-induced changes in the mechanical behavior of 3D printed polymers. *Composites Part C: Open Access*, *7*. https://doi.org/10.1016/j.jcomc.2022.100243
Bayer, I. S. (2023). Controlled Drug Release from Nanoengineered Polysaccharides. In *Pharmaceutics* (Vol. 15, Issue 5). MDPI. https://doi.org/10.3390/pharmaceutics15051364
Bukhovets, A. v., Fotaki, N., Khutoryanskiy, V. v., & Moustafine, R. I. (2020). Interpolymer complexes of eudragit® copolymers as novel carriers for colon-specific drug delivery. *Polymers*, *12*(7), 1–16. https://doi.org/10.3390/polym12071459
Cai, X., Wang, X., He, M., Wang, Y., Lan, M., Zhao, Y., & Gao, F. (2021). Colon-targeted delivery of tacrolimus using pH-responsive polymeric nanoparticles for murine colitis therapy. *International Journal of Pharmaceutics*, *606*. https://doi.org/10.1016/j.ijpharm.2021.120836
Carbinatto, F. M., de Castro, A. D., Evangelista, R. C., & Cury, B. S. F. (2014). Insights into the swelling process and drug release mechanisms from cross-linked pectin/high amylose starch matrices. *Asian Journal of Pharmaceutical Sciences*, *9*(1), 27–34. https://doi.org/10.1016/j.ajps.2013.12.002
Charbe, N., McCarron, P., Lane, M., & Tambuwala, M. (2017). Application of three-dimensional printing for colon targeted drug delivery systems. *International Journal of Pharmaceutical Investigation*, *7*(2), 47. https://doi.org/10.4103/jphi.jphi_32_17
Chen, J. K., Shen, C. R., & Liu, C. L. (2010). N-acetylglucosamine: Production and applications. In *Marine Drugs* (Vol. 8, Issue 9, pp. 2493–2516). MDPI AG. https://doi.org/10.3390/md8092493
Cochis, A., Bonetti, L., Sorrentino, R., Negrini, N. C., Grassi, F., Leigheb, M., Rimondini, L., & Farè, S. (2018). 3D printing of thermo-responsive methylcellulose hydrogels for cell-sheet engineering. *Materials*, *11*(4). https://doi.org/10.3390/ma11040579
Colpo, J. C., Pigatto, C., Brizuela, N., Aragón, J., & dos Santos, L. A. L. (2018). Antibiotic and anesthetic drug release from double-setting α-TCP cements. *Journal of Materials Science*, *53*(10), 7112–7124. https://doi.org/10.1007/s10853-018-2071-4
DeStefano, V., Khan, S., & Tabada, A. (2020). Applications of PLA in modern medicine. *Engineered Regeneration*, *1*, 76–87. https://doi.org/10.1016/j.engreg.2020.08.002
Dias, A. M., Correia, A., Pereira, M. S., Almeida, C. R., Alves, I., Pinto, V., Catarino, T. A., Mendes, N., Leander, M., Teresa Oliva-Teles, M., Maia, L., Delerue-Matos, C., Taniguchi, N., Lima, M., Pedroto, I., Marcos-Pinto, R., Lago, P., Reis, C. A., Vilanova, M., & Pinho, S. S. (2018). Metabolic control of T cell immune response through glycans in inflammatory bowel disease. *Proceedings of the National Academy of Sciences of the United States of America*, *115*(20), E4651–E4660. https://doi.org/10.1073/pnas.1720409115

Farrag, Y., Ide, W., Montero, B., Rico, M., Rodríguez-Llamazares, S., Barral, L., & Bouza, R. (2018). Preparation of starch nanoparticles loaded with quercetin using nanoprecipitation technique. *International Journal of Biological Macromolecules*, *114*, 426–433. https://doi.org/10.1016/j.ijbiomac.2018.03.134

Ferrero, C., Muñ Oz-Ruiz, A., & Jiménez-Castellanos, M. R. (2000). Fronts movement as a useful tool for hydrophilic matrix release mechanism elucidation. In *International Journal of Pharmaceutics* (Vol. 202). www.elsevier.com/locate/ijpharm

Filippone, G., Carroccio, S. C., Mendichi, R., Gioiella, L., Dintcheva, N. T., & Gambarotti, C. (2015). Time-resolved rheology as a tool to monitor the progress of polymer degradation in the melt state - Part I: Thermal and thermo-oxidative degradation of polyamide 11. *Polymer*, *72*, 134–141. https://doi.org/10.1016/j.polymer.2015.06.059

Goyanes, A., Buanz, A. B. M., Hatton, G. B., Gaisford, S., & Basit, A. W. (2015). 3D printing of modified-release aminosalicylate (4-ASA and 5-ASA) tablets. *European Journal of Pharmaceutics and Biopharmaceutics*, *89*, 157–162. https://doi.org/10.1016/j.ejpb.2014.12.003

Goyanes, A., Chang, H., Sedough, D., Hatton, G. B., Wang, J., Buanz, A., Gaisford, S., & Basit, A. W. (2015). Fabrication of controlled-release budesonide tablets via desktop (FDM) 3D printing. *International Journal of Pharmaceutics*, *496*(2), 414–420. https://doi.org/10.1016/j.ijpharm.2015.10.039

Heredia, N. S., Vizuete, K., Flores-Calero, M., Katherine Pazmiño, V., Pilaquinga, F., Kumar, B., & Debut, A. (2022). Comparative statistical analysis of the release kinetics models for nanoprecipitated drug delivery systems based on poly(lactic-co-glycolic acid). *PLoS ONE*, *17*(3 March). https://doi.org/10.1371/journal.pone.0264825

Horn, S. J., & Eijsink, V. G. H. (2004). A reliable reducing end assay for chito-oligosaccharides. *Carbohydrate Polymers*, *56*(1), 35–39. https://doi.org/10.1016/j.carbpol.2003.11.011

Huang, Y., Guo, W., Zhang, J., Peng, X., Li, G., Zhang, L. M., & Yang, L. (2020). Thermosensitive hydrogels based on methylcellulose derivatives for prevention of postoperative adhesion. *Cellulose*, *27*(3), 1555–1571. https://doi.org/10.1007/s10570-019-02857-4

Jiang, J., Han, X., Xu, H. (2021). Injectable Methylcellulose and Hyaluronic Acid Hydrogel containing silver nanoparticles for their effective anti-microbial and wound healing activity in nursing care for burn injuries in children. *Journal of Polymers and the Environment*. https://doi.org/10.21203/rs.3.rs-490312/v1

Lamichhane, S., Park, J. B., Sohn, D. H., & Lee, S. (2019). Customized novel design of 3D printed pregabalin tablets for intra-gastric floating and controlled release using fused deposition modeling. *Pharmaceutics*, *11*(11). https://doi.org/10.3390/pharmaceutics11110564

Lenz, J., Finke, J. H., Bunjes, H., Kwade, A., & Juhnke, M. (2021). Tablet formulation development focusing on the functional behaviour of water uptake and swelling. International Journal of Pharmaceutics: X, 3. https://doi.org/10.1016/j.ijpx.2021.100103

Linares, V., Casas, M., & Caraballo, I. (2019). Printfills: 3D printed systems combining fused deposition modeling and injection volume filling. Application to colon-specific drug delivery. *European Journal of Pharmaceutics and Biopharmaceutics*, *134*, 138–143. https://doi.org/10.1016/j.ejpb.2018.11.021

Liu, Z., & Yao, P. (2015). Injectable thermo-responsive hydrogel composed of xanthan gum and methylcellulose double networks with shear-thinning property. *Carbohydrate Polymers*, *132*, 490–498. https://doi.org/10.1016/j.carbpol.2015.06.013

Kontárová, S., Přikryl, R., Melčová, V., Menčík, P., Horálek, M., Figalla, S., Plavec, R., Feranc, J., Sadílek, J., & Pospíšilová, A. (2020). Printability, mechanical and thermal

properties of poly(3-hydroxybutyrate)-poly(lactic acid)-plasticizer blends for three-dimensional (3D) printing. *Materials*, *13*(21), 1–28. https://doi.org/10.3390/ma13214736
Ma, W. C., Lee, J. M., An, J., & Yeong, W. Y. (2022). 3D Printing in Triggered Drug Delivery Devices: A Review. *Biomedical Materials & Devices*. https://doi.org/10.1007/s44174-022-00058-5
Makhlof, A., Tozuka, Y., & Takeuchi, H. (2009a). pH-Sensitive nanospheres for colon-specific drug delivery in experimentally induced colitis rat model. *European Journal of Pharmaceutics and Biopharmaceutics*, *72*(1), 1–8. https://doi.org/10.1016/j.ejpb.2008.12.013
McCoubrey, L. E., Favaron, A., Awad, A., Orlu, M., Gaisford, S., & Basit, A. W. (2023). Colonic drug delivery: Formulating the next generation of colon-targeted therapeutics. In *Journal of Controlled Release* (Vol. 353, pp. 1107–1126). Elsevier B.V. https://doi.org/10.1016/j.jconrel.2022.12.029
Mirdamadian, S. Z., Varshosaz, J., Minaiyan, M., & Taheri, A. (2022). 3D printed tablets containing oxaliplatin loaded alginate nanoparticles for colon cancer targeted delivery. An in vitro/in vivo study. *International Journal of Biological Macromolecules*, *205*, 90–109. https://doi.org/10.1016/j.ijbiomac.2022.02.080
Moutaharrik, S., Maroni, A., Melocchi, A., Zema, L., Foppoli, A., Cerea, M., Palugan, L., Neut, C., Siepmann, F., Siepmann, J., & Gazzaniga, A. (2021). Oral colon delivery platform based on a novel combination approach: Design concept and preliminary evaluation. *Journal of Drug Delivery Science and Technology*, *66*. https://doi.org/10.1016/j.jddst.2021.102919
Narala, S., Nyavanandi, D., Mandati, P., Youssef, A. A. A., Alzahrani, A., Kolimi, P., Zhang, F., & Repka, M. (2023). Preparation and in vitro evaluation of hot-melt extruded pectin-based pellets containing ketoprofen for colon targeting. *International Journal of Pharmaceutics: X*, *5*. https://doi.org/10.1016/j.ijpx.2022.100156
Negim, E. S. M., Nurpeissova, Z. A., Mangazbayeva, R. A., Khatib, J. M., Williams, C., & Mun, G. A. (2014). Effect of pH on the physico-mechanical properties and miscibility of methyl cellulose/poly(acrylic acid) blends. In *Carbohydrate Polymers* (Vol. 101, Issue 1, pp. 415–422). Elsevier Ltd. https://doi.org/10.1016/j.carbpol.2013.09.047
Ou, Y. H., Goh, W. J., & Lim, S. H. (2023). Form & formulation approaches for COntRollable Release in 3D printed Colonic Targeting (CORR3CT) budesonide tablet. *International Journal of Pharmaceutics*, *635*. https://doi.org/10.1016/j.ijpharm.2023.122680
Pandey, M., Choudhury, H., Fern, J. L. C., Kee, A. T. K., Kou, J., Jing, J. L. J., Her, H. C., Yong, H. S., Ming, H. C., Bhattamisra, S. K., & Gorain, B. (2020). 3D printing for oral drug delivery: a new tool to customize drug delivery. *Drug Delivery and Translational Research*, *10*(4), 986–1001. https://doi.org/10.1007/s13346-020-00737-0
Peppas, N. A., & Sahlin, J. J. (1989). A simple equation for the description of solute release. III. Coupling of diffusion and relaxation. In *International Journal of Pharmaceutics* (Vol. 57).
Pereira, E. D., da Silva Dutra, L., Paiva, T. F., de Almeida Carvalho, L. L., Rocha, H. V. A., & Pinto, J. C. (2023). In Vitro Release and In Vivo Pharmacokinetics of Praziquantel Loaded in Different Polymer Particles. *Materials*, *16*(9). https://doi.org/10.3390/ma16093382
Pitzanti, G., Mathew, E., Andrews, G. P., Jones, D. S., & Lamprou, D. A. (2022). 3D Printing: an appealing technology for the manufacturing of solid oral dosage forms. In *The Journal of pharmacy and pharmacology* (Vol. 74, Issue 10, pp. 1427–1449). NLM (Medline). https://doi.org/10.1093/jpp/rgab136
Qu, Z., Wong, K. Y., Moniruzzaman, M., Begun, J., Santos, H. A., Hasnain, S. Z., Kumeria, T., McGuckin, M. A., & Popat, A. (2021). One-Pot Synthesis of pH-Responsive Eudragit-Mesoporous Silica Nanocomposites Enable Colonic Delivery of Glucocorticoids for the Treatment of Inflammatory Bowel Disease. *Advanced Therapeutics*, *4*(2). https://doi.org/10.1002/adtp.202000165

Ramot, Y., Haim-Zada, M., Domb, A. J., & Nyska, A. (2016). Biocompatibility and safety of PLA and its copolymers. In *Advanced Drug Delivery Reviews* (Vol. 107, pp. 153–162). Elsevier B.V. https://doi.org/10.1016/j.addr.2016.03.012

Ritger, P. L., & Peppas, N. A. (1987). A simple equation for description of solute release i. fickian and non-fickian release from non-swellable devices in the form of slabs, spheres, cylinders or discs. In *Journal of Controlled Release* (Vol. 5).

Rostamitabar, M., Subrahmanyam, R., Gurikov, P., Seide, G., Jockenhoevel, S., & Ghazanfari, S. (2021). Cellulose aerogel micro fibers for drug delivery applications. *Materials Science and Engineering C*, *127*. https://doi.org/10.1016/j.msec.2021.112196

Sadia, M., Arafat, B., Ahmed, W., Forbes, R. T., & Alhnan, M. A. (2018). Channelled tablets: An innovative approach to accelerating drug release from 3D printed tablets. *Journal of Controlled Release*, *269*, 355–363. https://doi.org/10.1016/j.jconrel.2017.11.022

Schmitz, C. (2021). *Development of a fully enzymatic conversion process from marine chitin to chitosan oligomers* [maastricht university]. https://doi.org/10.26481/dis.20211103cs

Siepmann, J., & Peppas, N. A. (2012). Modeling of drug release from delivery systems based on hydroxypropyl methylcellulose (HPMC). In *Advanced Drug Delivery Reviews* (Vol. 64, Issue SUPPL., pp. 163–174). https://doi.org/10.1016/j.addr.2012.09.028

Tabassum, N., Ahmed, S., & Ali, M. A. (2021). Chitooligosaccharides and their structural-functional effect on hydrogels: A review. In Carbohydrate Polymers (Vol. 261). Elsevier Ltd. https://doi.org/10.1016/j.carbpol.2021.117882

Talukder, R. M., & Fassihi, R. (2008). Development and in-vitro evaluation of a colon-specific controlled release drug delivery system. *Journal of Pharmacy and Pharmacology*, *60*(10), 1297–1303. https://doi.org/10.1211/jpp/60.10.0005

Tannergren, C., Bergendal, A., Lennernäs, H., & Abrahamsson, B. (2009). Toward an increased understanding of the barriers to colonic drug absorption in humans: implications for early controlled release candidate assessment. *Molecular Pharmaceutics*, *6*(1), 60–73. https://doi.org/10.1021/mp800261a

Tate, M. C., Shear, D. A., Hoffmann, S. W., Stein, D. G., & Laplaca, M. C. (2001). Biocompatibility of methylcellulose-based constructs designed for intracerebral gelation following experimental traumatic brain injury. In *Biomaterials* (Vol. 22).

Unagolla, J. M., & Jayasuriya, A. C. (2018). Drug transport mechanisms and in vitro release kinetics of vancomycin encapsulated chitosan-alginate polyelectrolyte microparticles as a controlled drug delivery system. *European Journal of Pharmaceutical Sciences*, *114*, 199–209. https://doi.org/10.1016/j.ejps.2017.12.012

Vaz, V. M., & Kumar, L. (2021). 3D Printing as a Promising Tool in Personalized Medicine. In *AAPS PharmSciTech* (Vol. 22, Issue 1). Springer Science and Business Media Deutschland GmbH. https://doi.org/10.1208/s12249-020-01905-8

Veerareddy, P. R., & Vemula, S. K. (2012). Formulation, evaluation and pharmacokinetics of colon targeted pulsatile system of flurbiprofen. *Journal of Drug Targeting*, *20*(8), 703–714. https://doi.org/10.3109/1061186X.2012.712131

Vert, M. (2015). After soft tissues, bone, drug delivery and packaging, PLA aims at blood. *European Polymer Journal*, *68*, 516–525. https://doi.org/10.1016/j.eurpolymj.2015.03.051

Vemula, S. K. (2015a). Colon specific drug delivery: Effect of Eudragit enteric coating on hydroxypropyl methylcellulose matrix tablets of flurbiprofen. *Journal of Young Pharmacists*, *7*(4), 373–383. https://doi.org/10.5530/jyp.2015.4.12

Vemula, S. K. (2015b). Formulation and pharmacokinetics of colon-specific double-compression coated mini-tablets: Chronopharmaceutical delivery of ketorolac tromethamine. *International Journal of Pharmaceutics*, *491*(1–2), 35–41. https://doi.org/10.1016/j.ijpharm.2015.06.007

Vemula, S. K., & Veerareddy, P. R. (2013). Development, evaluation and pharmacokinetics of time-dependent ketorolac tromethamine tablets. Expert Opinion on Drug Delivery, 10(1), 33–45. https://doi.org/10.1517/17425247.2013.743528
Wilkes, G. L. (1981). *An Overview of the Basic Rheological Behavior of Polymer Fluids with an Emphasis on Polymer Melts*. https://doi.org/10.1021/ed058p880
Windolf, H., Chamberlain, R., & Quodbach, J. (2021). Predicting drug release from 3D printed oral medicines based on the surface area to volume ratio of tablet geometry. *Pharmaceutics*, *13*(9). https://doi.org/10.3390/pharmaceutics13091453
Wójcik-Pastuszka, D., Krzak, J., Macikowski, B., Berkowski, R., Osiński, B., & Musiał, W. (2019). Evaluation of the release kinetics of a pharmacologically active substance from model intra-articular implants replacing the cruciate ligaments of the knee. *Materials*, *12*(8). https://doi.org/10.3390/ma12081202
Zhang, F. (2016). Melt-Extruded Eudragit® FS-Based Granules for Colonic Drug Delivery. *AAPS PharmSciTech*, *17*(1), 56–67. https://doi.org/10.1208/s12249-015-0357-2

**Tables:**

**Table 1.** Prepared samples and their label

| **Sample information** | **Label** |
|---|---|
| 3D printed tablets with EURFS100/PLA (80/20 w/w) containing 100 µL GlcNAc (30 mg/ml)-loaded MC 3% (w/v) gel | EURFS100/PLA (80/20 w/w)-MC 3% w/v |
| 3D printed tablets with EURFS100/PLA (70/30 w/w) containing 100 µL GlcNAc (30 mg/ml)-loaded MC 3% (w/v) gel | EURFS100/PLA (70/30 w/w)-MC 3% w/v |
| 3D printed tablets with EURFS100/PLA (80/20 w/w) containing 100 µL GlcNAc (30 mg/ml)-loaded MC 2% (w/v) gel | EURFS100/PLA (80/20 w/w)-MC 2% w/v |
| 3D printed tablets with EURFS100/PLA (70/30 w/w) containing 100 µL GlcNAc (30 mg/ml)-loaded MC 2% (w/v) gel | EURFS100/PLA (70/30 w/w)-MC 2% w/v |

**Table 2.** Experimental design to determine the optimal parameters for the fabrication of the 3D printed tablets

| | **Experiment 1: Effect of polymer ratio on 3D printed tablets** | **Experiment 2: Effect of MC concentration on 3D printed tablets** |
|---|---|---|
| **Polymer ratio** | EURFS100/PLA (80/20 w/w, 70/30 w/w) | EURFS100/PLA (80/20 w/w) |
| **MC concentration** | 3% w/v | 3% w/v<br>2% w/v |
| **Read outs** | Printability and processability | Processability |
| | Physical characteristics of tablets | Physical characteristics of tablets |
| | Drug Release | Drug Release |

**Table 3.** Characterization of the diffusion exponent n based on the geometry of the dosage form

| **Thin Film Mechanism** | **Cylinder** | **Sphere** | **Drug Release** |
|---|---|---|---|
| 0.50 | 0.45 | 0.43 | Fickian diffusion |
| 0.50 < n < 1.00 | 0.45 < n < 0.89 | 0.43 < n < 0.85 | Anomalous transport |
| 1.00 | 0.89 | 0.85 | Case-II transport |

**Table 4.** Composition of polymer blends and the printing outcome

| **Sample name** | **EURFS100 (W%)** | **PLA (W%)** | **Results** |
|---|---|---|---|
| EURFS100/PLA (60/40) | 60 | 40 | Separation of the polymer blends |
| EURFS100/PLA (70/30) | 70 | 30 | Printing inconsistency |
| EURFS100/PLA (80/20) | 80 | 20 | Great printing and consistent production |

**Table 5.** Printing design parameters for different sections of the tablet

| **Sample name** | **Middle Infill (%)** | **Top/bottom infill (%)** | **Discharge** | **Results** |
|---|---|---|---|---|
| Design-1 | 20 | 60 | 80 | Gel leakage |

| | | | | |
|---|---|---|---|---|
| Design-2 | 20 | 80 | 80 | Good gel injection and sealing |
| Design-3 | 40 | 80 | 80 | Impossible to inject the gel |

**Table 6.** The rate constant, and $R^2$ values of the Higuchi model.

| **Sample** | $\boldsymbol{k}$ | $\boldsymbol{R^2}$ |
|---|---|---|
| EURFS100/PLA (80/20 w/w)-MC 3% w/v | 12.60 | 0.90 |
| EURFS100/PLA (70/30 w/w)-MC 3% w/v | 7.09 | 0.84 |
| EURFS100/PLA (80/20 w/w)-MC 2% w/v | 16.98 | 0.91 |
| EURFS100/PLA (70/30 w/w)-MC 2% w/v | 9.14 | 0.82 |

**Table 7.** The rate constant, release exponent, and $R^2$ values of the Korsmeyer-Peppas model.

| **Sample** | $\boldsymbol{k}$ | $\boldsymbol{n}$ | $\boldsymbol{R^2}$ |
|---|---|---|---|
| EURFS100/PLA (80/20 w/w)-MC 3% w/v | 6.27 | 0.84 | 0.97 |
| EURFS100/PLA (70/30 w/w)-MC 3% w/v | 0.15 | 1.74 | 0.96 |
| EURFS100/PLA (80/20 w/w)-MC 2% w/v | 13.32 | 0.66 | 0.94 |
| EURFS100/PLA (70/30 w/w)-MC 2% w/v | 0.45 | 1.76 | 0.91 |

**Table 8.** $k_d$, $k_r$, and r values of the Peppas-Sahlin model.

| **Sample** | $\boldsymbol{k_d}$ | $\boldsymbol{k_r}$ | $\boldsymbol{R^2}$ |
|---|---|---|---|
| EURFS100/PLA (80/20 w/w)-MC 3% w/v | -22.40 | 12.98 | 0.996 |
| EURFS100/PLA (70/30 w/w)-MC 3% w/v | -19.15 | 6.52 | 0.994 |
| EURFS100/PLA (80/20 w/w)-MC 2% w/v | -15.34 | 14.89 | 0.988 |
| EURFS100/PLA (70/30 w/w)-MC 2% w/v | -18.14 | 9.34 | 0.978 |

**Table 9.** Calculated values of MDT, T10%, and T80%.

| **Sample** | **MDT (h)** | **T10% d(h)** | **T80% d(h)** |
|---|---|---|---|
| EURFS100/PLA (80/20 w/w)-MC 3% w/v | 11.43 | 4.22 | 20 |
| EURFS100/PLA (70/30 w/w)-MC 3% w/v | 18.22 | 9.41 | >24 |
| EURFS100/PLA (80/20 w/w)-MC 2% w/v | 9.35 | 3.05 | 14 |
| EURFS100/PLA (70/30 w/w)-MC 2% w/v | 15.08 | 5.13 | 23.1 |

**Figures:**

**Figure 1.** The chemical structure of MC (A) and GlcNAc (B) created by ChemDraw.

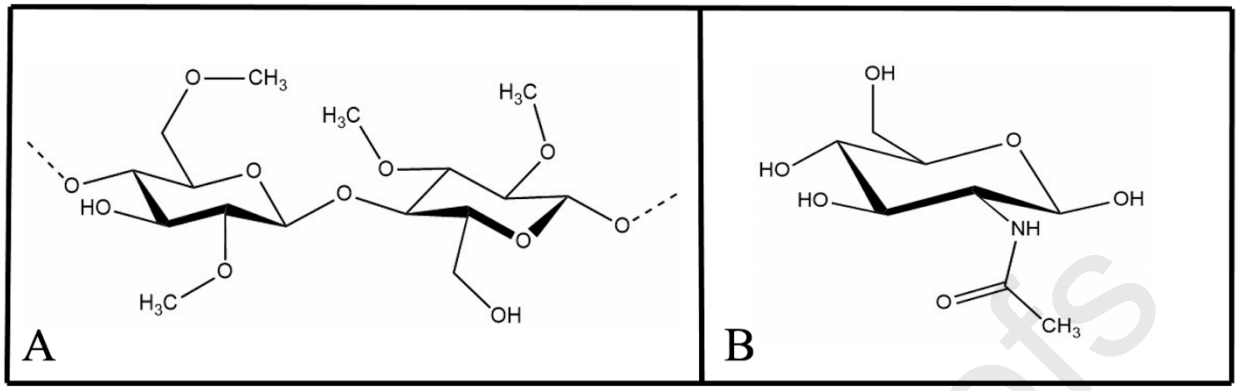


**Figure 2.** The chemical structure of EURFS100 (A) and PLA (B) created by ChemDraw.

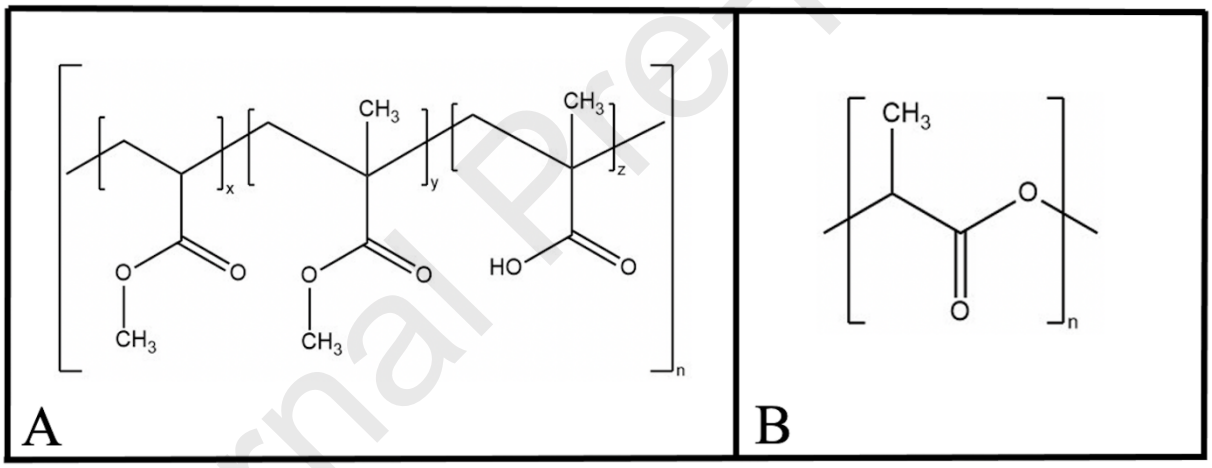


**Figure 3.** A) Arburg 200-3X 3D printer created by Cura software. (B) Illustration of various temperature zones representing how the polymer blend is subjected to various temperatures in different units during the printing process.

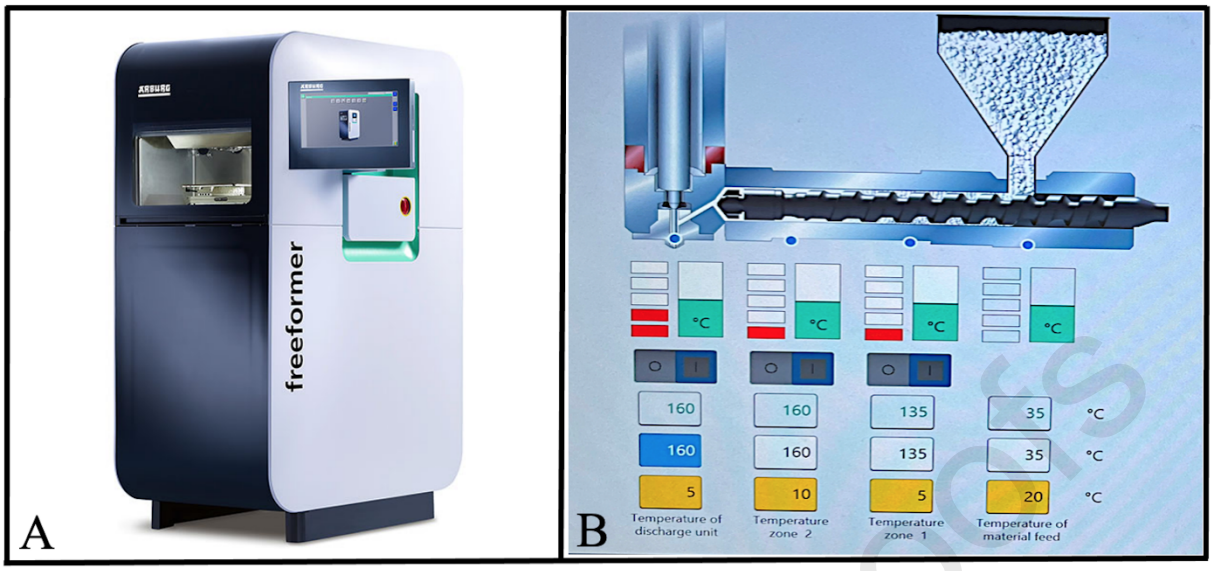


**Figure 4.** Schematic view of 3D printing process. A) Printing the bottom layers and a part of the middle layers of the tablet, B) injecting the (drug-loaded) gel, and C) printing the remaining part of the tablet. "Graphical elements were created with BioRender.com".

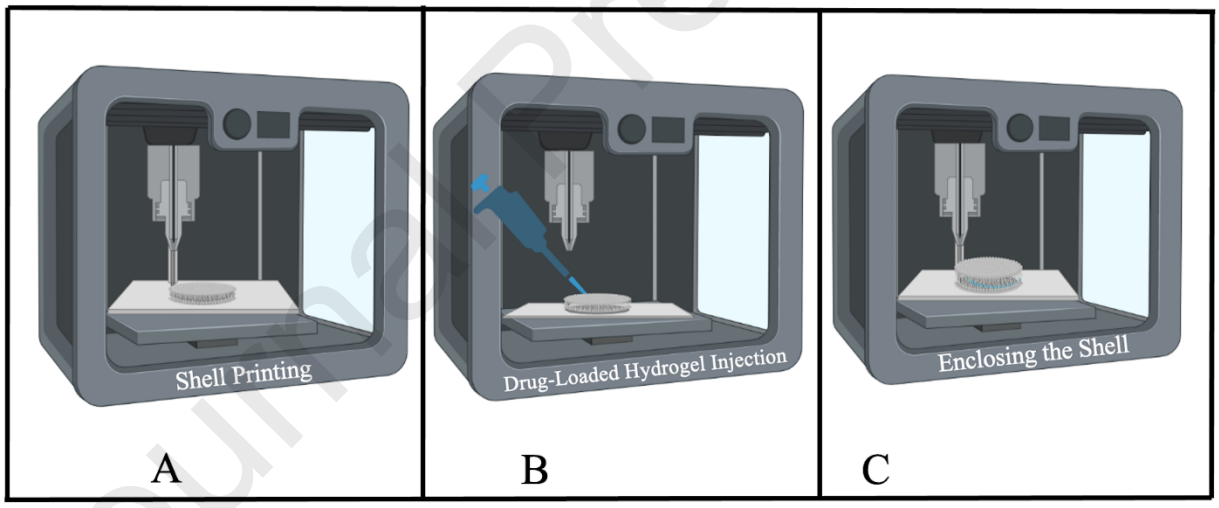


**Figure 5.** A) Optimum droplet size visualized and measured after printing a shell. B) The tablet′s final design (upper image), including the top, middle, and bottom layers (lower image) created by SolidWorks software.

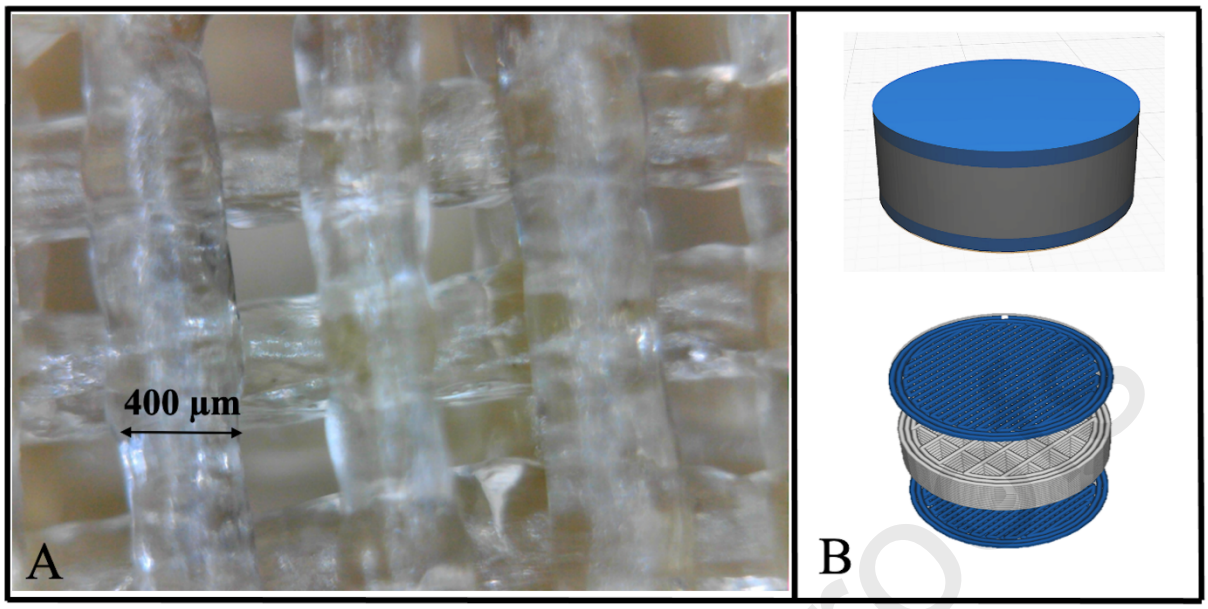


**Figure 6.** Physical characteristics of the tablets under various circumstances. (A) Three 3D printed tablets prior to drug release experiment (B) Weight of the 3D printed tablets. (C) Thickness of the 3D printed tablets. (D) Diameter of 3D printed tablets. Data are shown as mean ± SD. ** = $p \leq 0.01$, **** = $p \leq 0.0001$ (* data statistically significantly different)

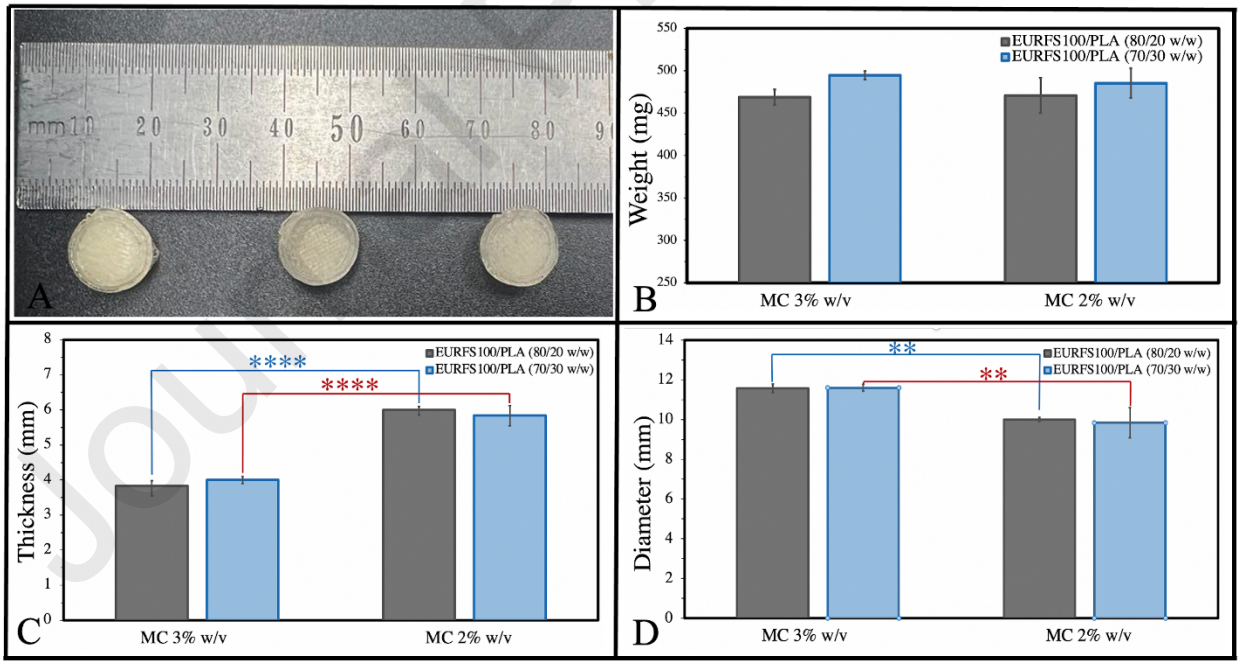


**Figure 7.** SEM images of tablets. (A) A 3D printed tablet image displaying the whole view of tablets, (B) a center view of the top layer surface showing a few unmelted polymeric spots, and (C) an edge view revealing the tablet's slightly uneven surface.

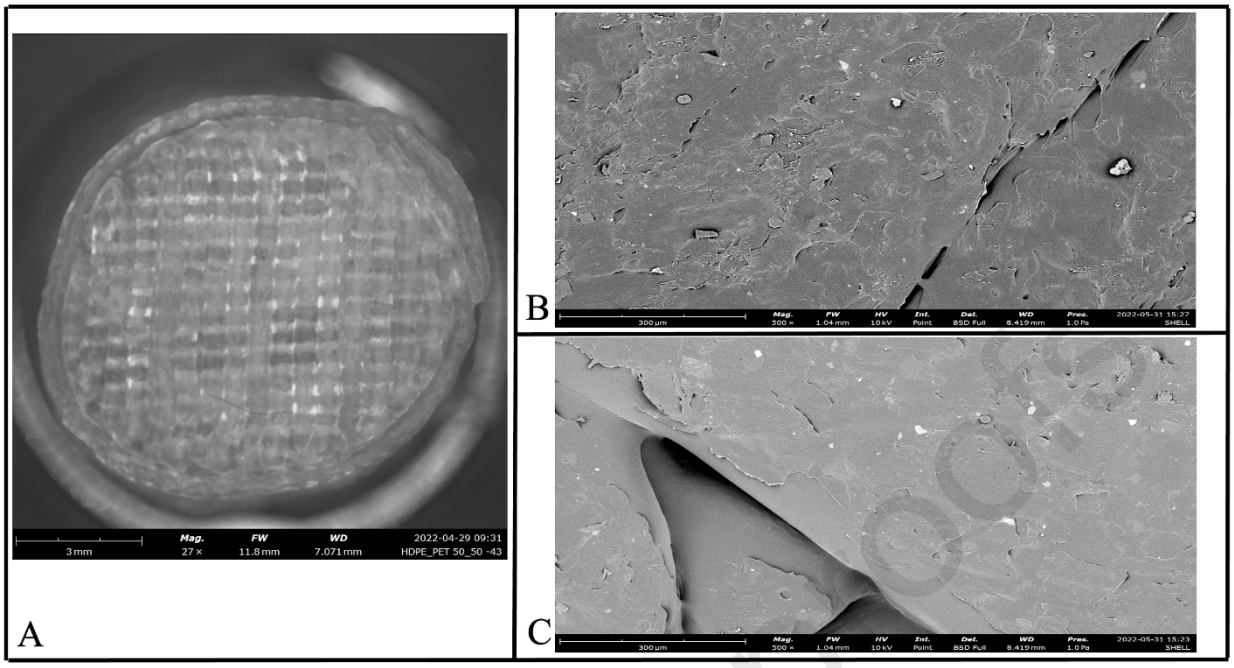


**Figure 8.** Rheology of the MC hydrogels. A) G′ and G″ as a function of angular frequency at two different temperatures, showing close values for G' and G" across the low angular frequency ramp, and B) viscosity as a function of shear rate, both gels show shear thinning behaviors.

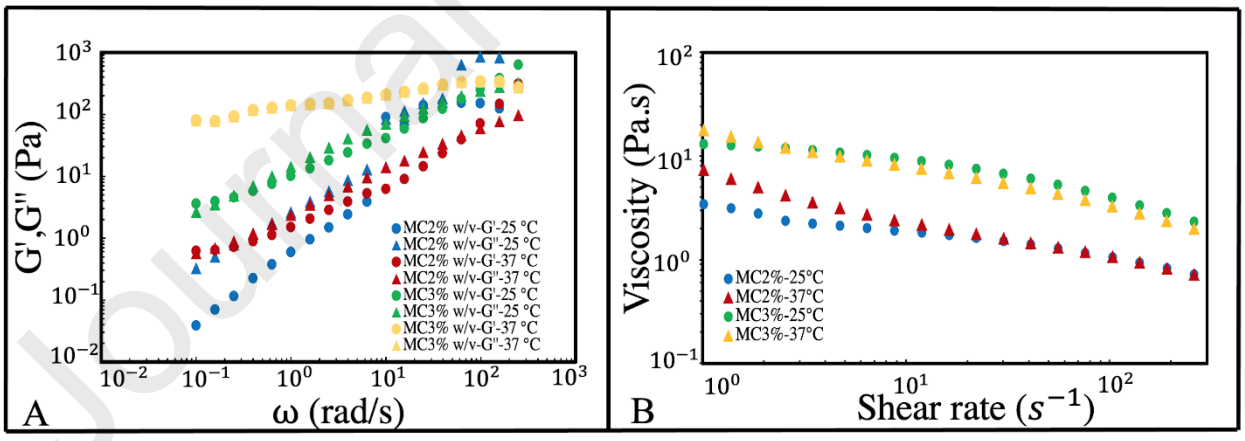


**Figure 9.** Time evolution of G′ and G″ of Eudragit FS100 (A), PLA (B), Eudragit FS100/PLA (80/20 w/w) (C), and Eudragit FS100/PLA (70/30 w/w) (D) at various angular frequencies, showing the degradation process of these polymers in response to time at a fixed temperature of 160 °C.

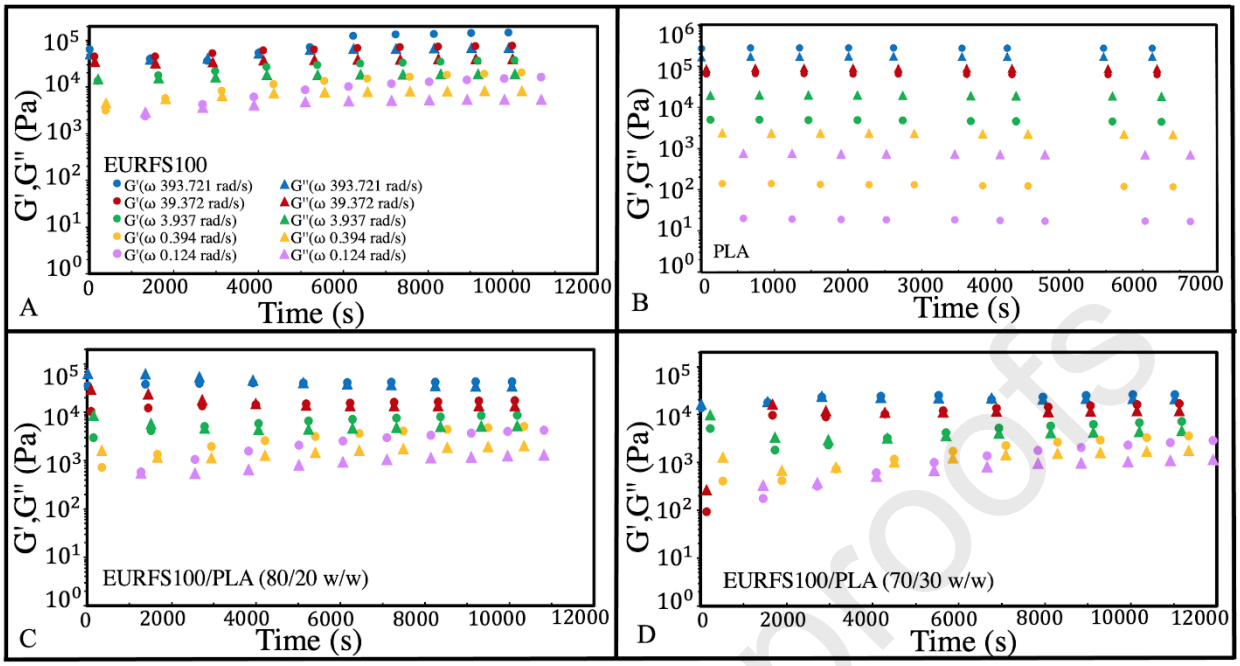


**Figure 10.** A) TGA graphs of the EURFS100, PLA, and polymer blends. The step from 180 to 200 °C in the mass loss was due to the evaporation of some volatiles in the structure. B) DTA of the polymer blends showed that the decomposition range was broader and the rate was slower in the ratio of 20% PLA.

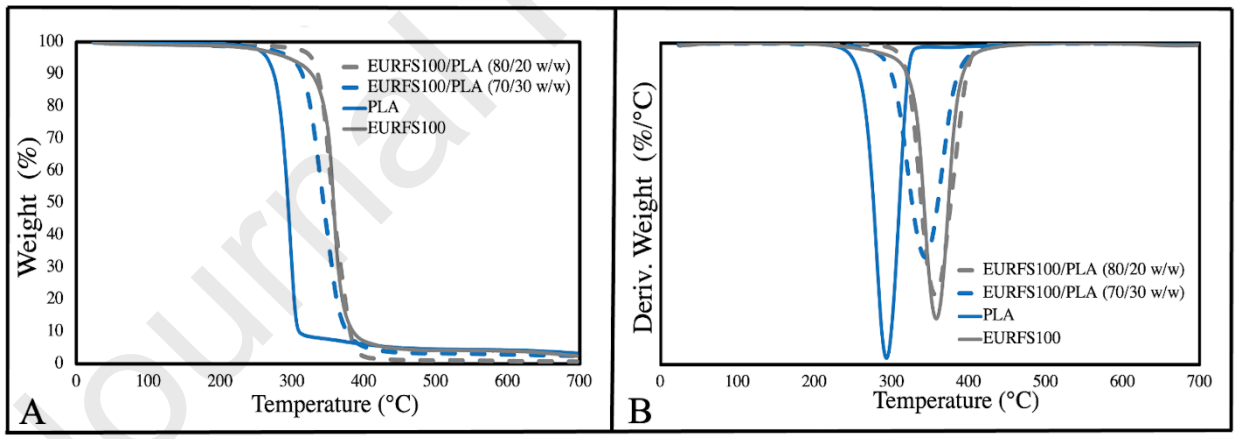


**Figure 11.** DSC graphs (Exo up) of polymers showing the heating (A) and cooling (B) phases. The graph is displaying Tg values for various polymer blends and confirming the amorphous structure of the polymers; there is another endothermic event in the polymer

blends and EURFS100 starting at 170 °C with a mild baseline shift attributed to the evaporation of some volatiles.

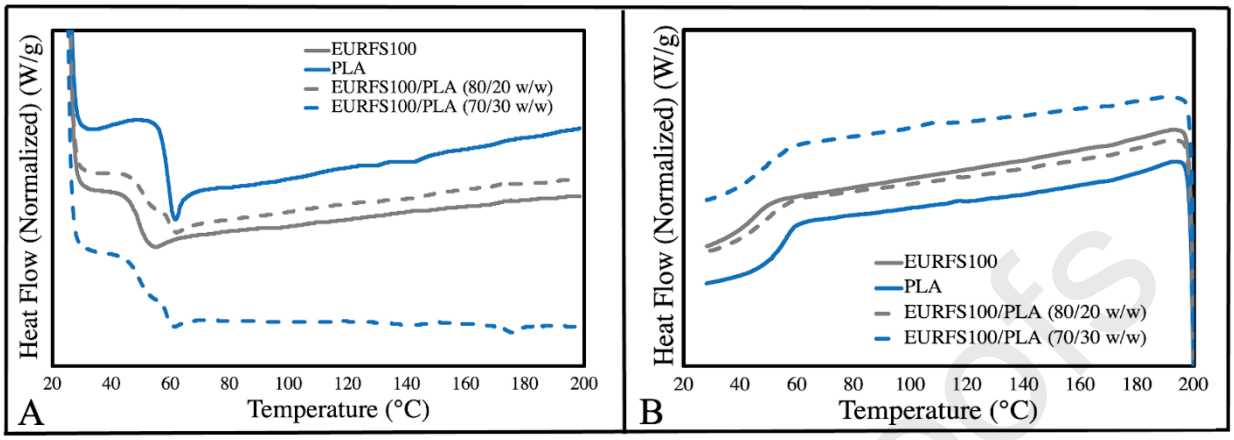


**Figure 12.** A) The cumulative release profile of GlcNAc under various conditions revealed sustained drug release, particularly for tablets containing MC 3% w/v, (B) GlcNAc content in 3D printed tablets showed no significant variations between the samples, and (C) 3D printed tablets maintained their shape after the release experiment. Data are shown as the mean ± SD.

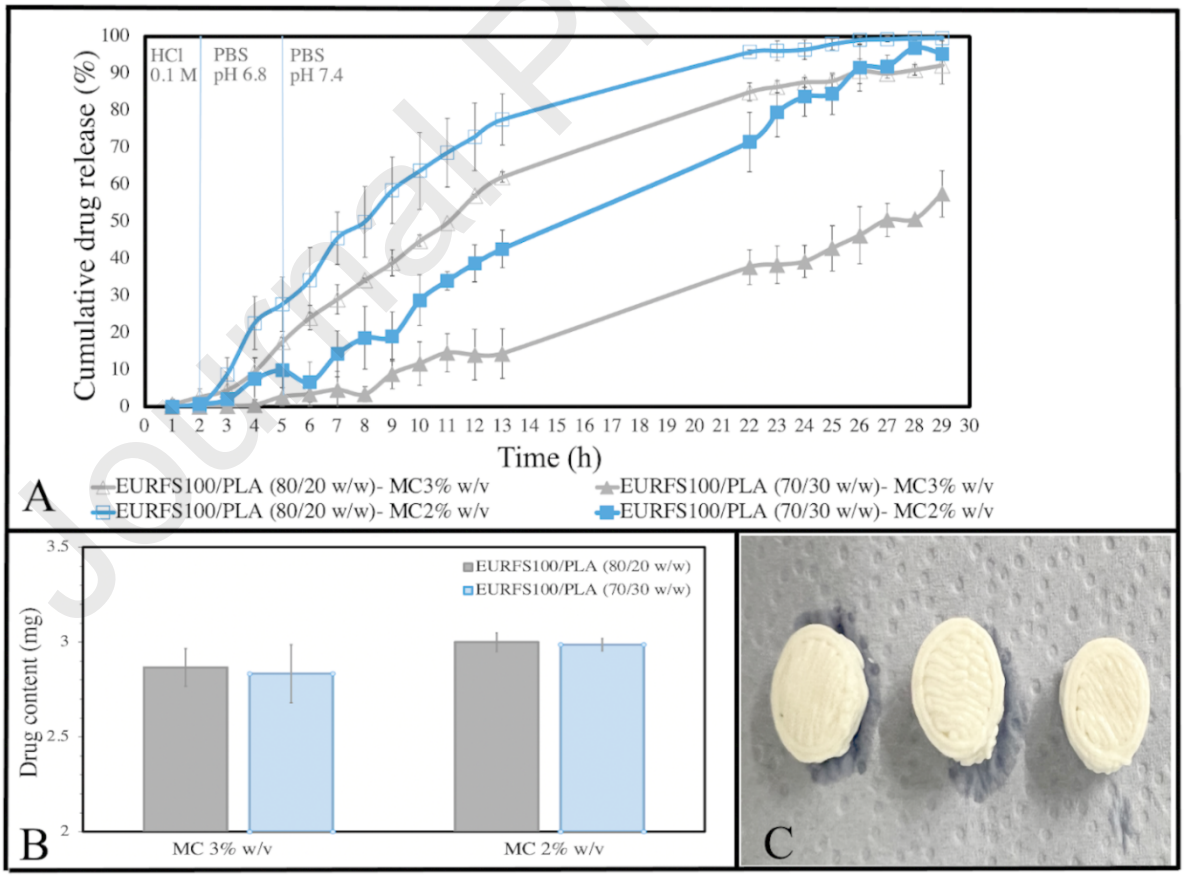

**Figure 13.** The R/F values in the Peppas-Sahlin model change over time. It is evident that these values are consistently greater than 1, suggesting that, except for the initial stages of the release experiment, polymer relaxation primarily governs the drug release mechanism.

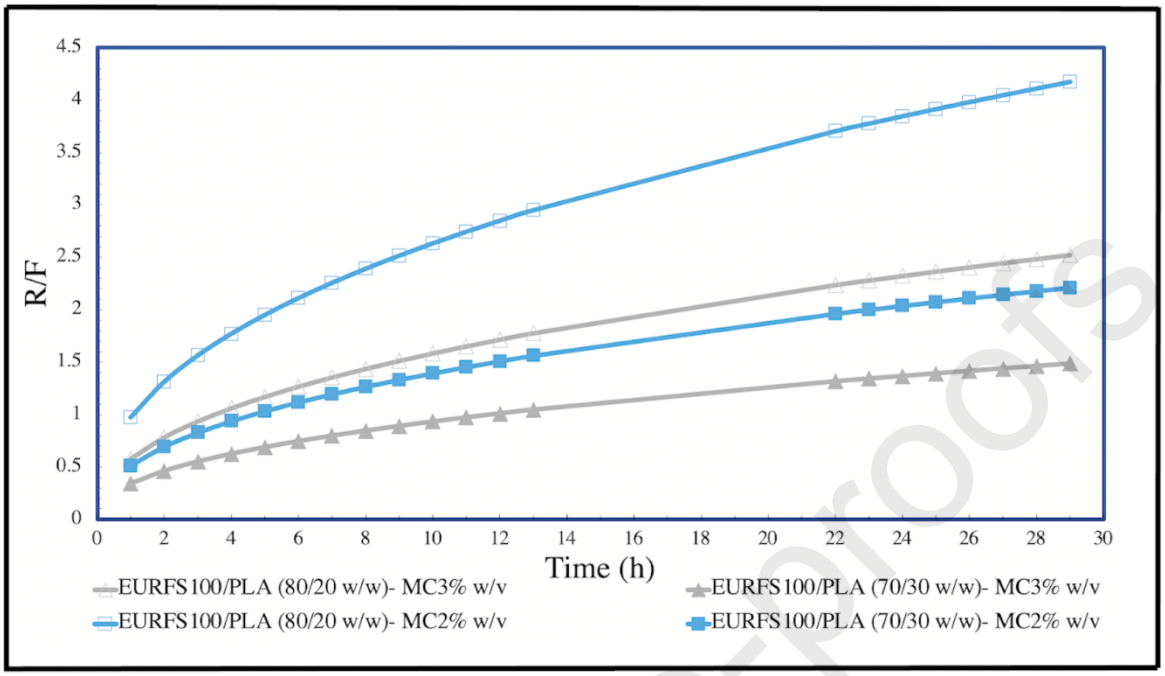


**Figure 14.** A) Schematic representation of XTT assay showing the sample preparation, created by "BioRender.com". XTT results of B) 3D printed samples, (C) MC hydrogels, and (D) GlcNAc solutions; cell viability was observed in the samples on day 1 of the experiment. The negative sample was DMEM and the positive one was DMSO. Data are shown as the mean ± SD. **** = $p \leq 0.0001$ (* data statistically significantly different)

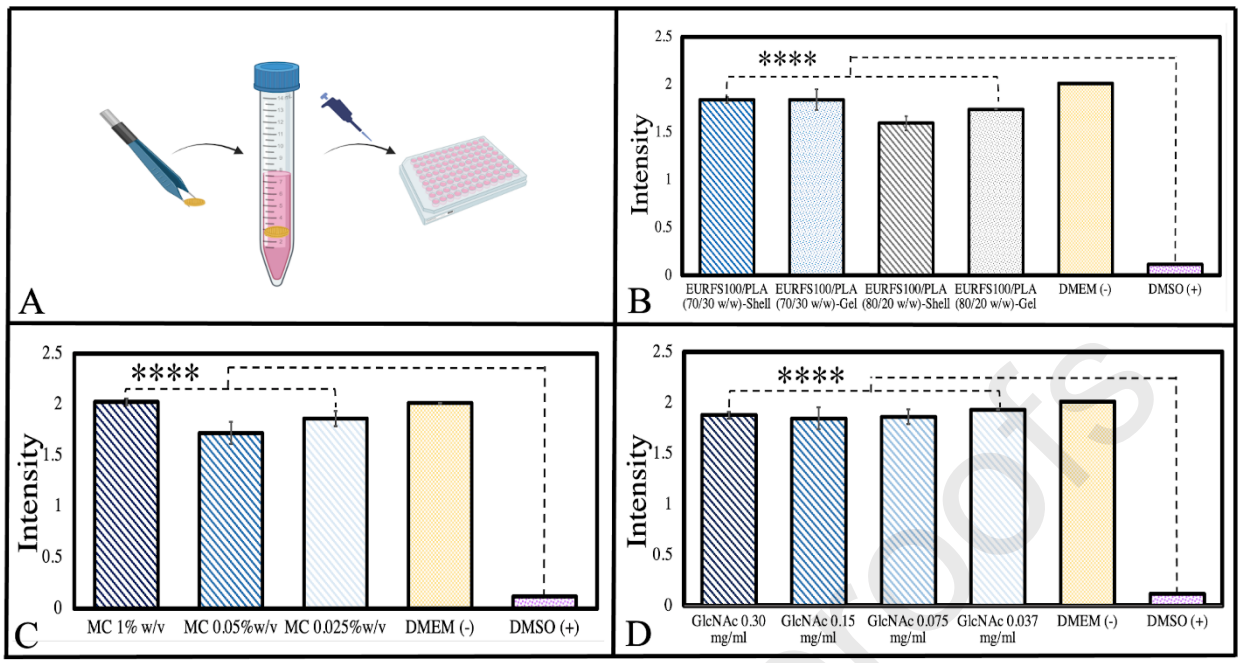

Graphical Abstract:

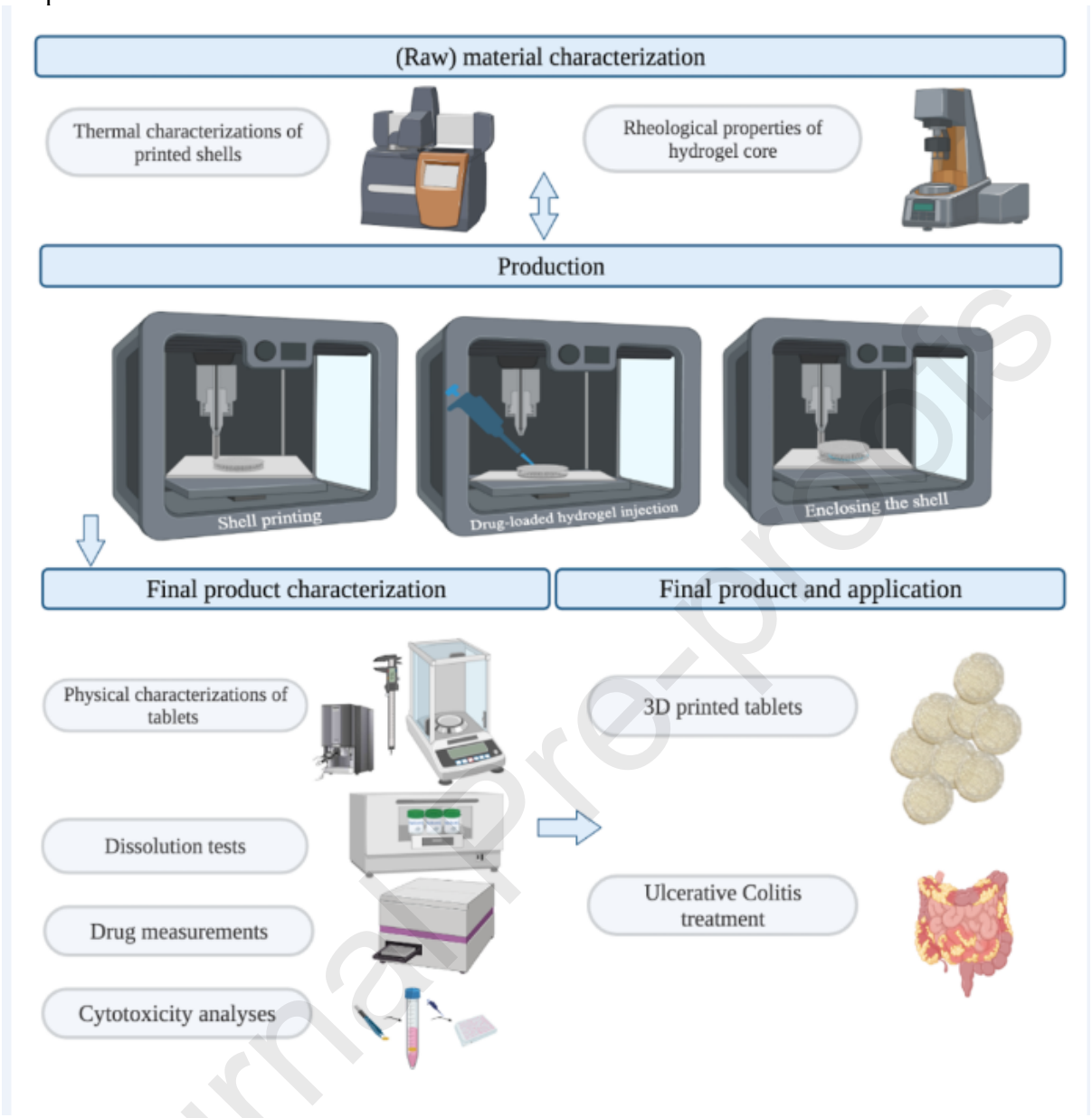

**Author Contributions:**
**Maryam Asadi:** Conceptualization, Methodology, Investigation, Validation, Visualization, Writing - Original draft. **Zeinab Salehi:** Conceptualization, Supervision, Reviewing and Editing. **Mohammad Akrami:** Conceptualization, Supervision, Reviewing and Editing. **Stefan Jockenhoevel:** Conceptualization. **Samaneh Ghazanfari:** Conceptualization, Investigation, Methodology, Project administration, Resources, Supervision, Validation, Writing - Review & Editing.

**Declaration of interests**

☒ The authors declare that they have no known competing financial interests or personal relationships that could have appeared to influence the work reported in this paper.

☐ The authors declare the following financial interests/personal relationships which may be considered as potential competing interests: